DOI: 10.1002/ejoc.200901175

Engineering Solid-State Molecular Switches: *N*-Salicylidene N-Heterocycle Derivatives

François Robert,[a] Anil D. Naik,[a] Florence Hidara,[a] Bernard Tinant,[b] Raphaël Robiette,[c] Johan Wouters,[d] and Yann Garcia*[a]

Keywords: Molecular devices / Thermochromism / Photochromism / Crystal engineering

A supramolecular engineering approach has been developed for a novel family of *N*-salicylidene aniline derivatives to control their thermo- and photochromic behaviours. Hsaltrz, Habs, Hsalphen, Hsaltz and Ksaltz are versatile molecules built from N-heterocycles, which drive the molecular arrangement to form a controlled crystal packing with predesigned optical properties. A complete structural, optical and computational study of powders of these new molecular nanoswitches is presented. An *N*-salicylidene aniline derivative possessing no thermo- or photoinduced chromic properties thanks to a specific molecular geometry was sought, and Habs and Hsalphen were designed to enhance π–π stacking interactions. A theoretical study of the crystal packing, combined with time-dependent diffuse reflectance studies of Habs, have confirmed the appearance of photochromism at room temperature completed with an unprecedented "spring-type effect" observed during the photochemical relaxation of the metastable *trans*-keto form. The absence of thermochromism in an *N*-salicylidene aniline derivative, induced by the absence of *cis*-keto form, is a unique behaviour, firstly identified and explained for these types of compounds. Finally, Hsaltz and Ksaltz are the result of a molecular derivation of Hsaltrz which allow enhancing the amplitude of thermochromism of these functional materials.

Introduction

Supramolecular chemistry constitutes a highly versatile research field where new complex chemical systems are made from simple components interacting through noncovalent intermolecular forces.[1] Supramolecular chemistry concepts have been largely used in materials science,[2] polymer science[3] and biology[4] and provide novel types of applications (solid-state receptors,[5] chemoresponsive sensors,[6] zeolite analogs,[7] etc). Supramolecular architectures are constructed thanks to steric and electronic information contained in basic molecular building blocks.[8] These primary covalent units are made of an internal algorithm that controls the final supramolecular assembly.[1] In such architectures, molecular entities (made by covalent bonds) are connected through a large panel of supramolecular interactions such as H-bonds,[9] π–π stackings,[10] hydrophilic,[11] ionic[12] and halogen–halogen interactions.[13] This diversity of interactions explains the complexity of supramolecules which can be either artificial (nanogrids,[14–16] nanoracks,[17] nanocages[18]) or natural[19] (DNA, recognition proteins). Supramolecular interactions can be very stable (thermodynamic) or very labile (kinetic),[20] which allows the system to (re)organize either itself[21] or under a given constraint (temperature,[21] light irradiation,[10,22] pH[23] and solvent change,[21] concentration[21]) to form complex self-assemblies. The self-reorganization ability of supramolecular systems plays also an important role in molecular recognition encountered in some host–guest complexes.[20] The nature of the supramolecular architecture can also be used to predict physical properties (cooperativity and spin-transition temperature,[24] magnetic behaviours,[16] porosity,[25] etc.) thanks to crystal structure control. This approach, called crystal engineering,[26] based on supramolecular chemistry concepts, allows simplifying the complex problem of structure prediction into a problem of network architecture[26] where molecules, metals, ions and so on are considered as nodes and the intermolecular interactions or coordination bonds represent node connections. In this report, we make use of this strategy to obtain new switchable functional materials based on the *N*-salicylidene moiety, whose optical properties could be finely tuned thanks to a proper electronic and structural control.

[a] Unité de Chimie des Matériaux Inorganiques et Organiques, Département de Chimie, Université Catholique de Louvain, Place L. Pasteur 1, 1348 Louvain-la-Neuve, Belgium
Fax: +32-1047-2330
E-mail: yann.garcia@uclouvain.be
[b] Unité de Chimie Structurale et des Mécanismes Réactionnels, Département de Chimie, Université Catholique de Louvain, Place L. Pasteur 1, 1348 Louvain-la-Neuve, Belgium
[c] Unité de Chimie Organique et Médicinale, Département de Chimie, Université Catholique de Louvain, Place L. Pasteur 1, 1348 Louvain-la-Neuve, Belgium
[d] Laboratoire de Chimie biologique Structurale, Faculté des Sciences, Facultés Notre-Dame de la Paix, Rue de Bruxelles 61, 5000 Namur, Belgium
Supporting information for this article is available on the WWW under http://dx.doi.org/10.1002/ejoc.200901175.

N-Salicylidene aniline derivatives have been used in various fields such as nonlinear optics,[27] catalysis,[28] biology[29] and several applications have been proposed (chemical sensor,[30] stimuli responsive polymer,[31] molecular machines,[32] information storage and display[33,34]). This latter application is probably the most promising one thanks to the thermo- and photochromism switching ability of a few *N*-salicylidene aniline derivatives[35] that occurs in the solid state and without fatigue.[36] Thermochromism, which corresponds to a temperature-induced reversible colour change,[37] is observed with a thermal tautomeric equilibrium between the uncoloured enol and the yellow *cis*-keto forms (Figure 1a). Photochromism, which is a similar optical phenomenon induced by light irradiation,[37] arises from photoisomerization of both the enol and *cis*-keto forms (Figure 1a) to the red *trans*-keto form. For *N*-salicylidene aniline, photochromism is induced by light irradiation at 365 and 436 nm but derivatives can absorb at others wavelengths, as demonstrated by the large range of colours shown by these molecules.[38] The photochemical process associated to the photochromism has been described.[39–41] UV irradiation (Figure 1b) of the enol form leads to the formation of the excited enol form (enol*). This species can fluoresce in the visible region in some rare cases[42] or complete a fast tautomerization to the excited *cis*-keto form (*cis**). The *cis** to *cis* relaxation is mainly radiative and is always detected by fluorescence spectroscopy.[38] The *cis** form can also undergoes photoisomerization to produce the excited *trans*-keto (*trans**), which is described to be non-fluorescent. It is assumed that the *trans**–*trans* relaxation is mostly nonradiative. Back reaction from *trans*-keto to *cis*-keto and enol forms is either thermally or photochemically induced. The thermal lifetime of the metastable *trans*-keto form strongly depends on the energy barrier between the *trans*- and *cis*-keto forms and leads to a fast or slow thermal relaxation.[42]

N-Salicylidene aniline derivatives are not the only possible candidates for light-induced information storage applications. Many others photochromic molecules have been described by using a large range of chemical reaction such as redox reactions,[43] electron-hole pair generation,[44] spin crossover,[45] coordination change,[46] photocyclization,[43] photoisomerization,[47] bond cleavage[48] and so on. Nevertheless, solid-state photochromism appears to be rare and only a few systems fulfill criteria for data storage applications. A good thermal stability, low fatigue, rapid response and nondestructive readout capability of switchable forms are indeed necessary.[49] *N*-Salicylidene aniline derivatives are promising candidates but to fulfill these application requirements, optical and structural properties of these molecules must be accurately controlled and hence fully understood.

N-Salicylidene aniline derivatives were firstly claimed to be thermochromic or photochromic but not both.[38,50,51] This exclusive classification was recently clarified[35] and *N*-salicylidene aniline derivatives were shown to be either photochromic and thermochromic or only thermochromic (except for few rare examples that are neither thermo- nor

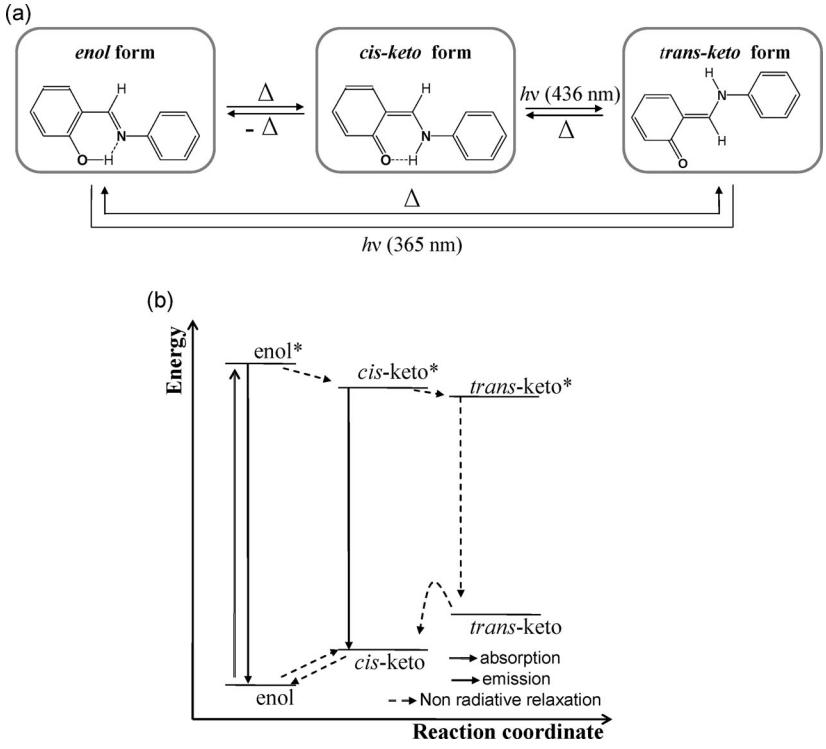

Figure 1. (a) Thermochromism and photochromism of *N*-salicylidene aniline. (b) Photochemical process leading to the formation of the *trans*-keto form from the enol form for *N*-salicylidene aniline.

photochromic, which present a strong deep red coloration[38] probably originating from a very large *cis*-keto form population). Being aware of the importance to predict these optical properties, a structure–properties classification was proposed.[51] Thermochromic compounds were observed as very planar molecules that are closely packed in the crystal lattice, with a low dihedral angle between aromatic rings ($\Phi < 25°$). These structures are stabilized by strong π–π or CH–π supramolecular interactions. Aromatic rings and imine groups are particularly involved in these interactions, assisted by charge-transfer phenomenon.[52] A typical example of this type of packing is represented by the *N*-salicylidene 2-aminopyridine crystal structure.[51,53] Thermo- and photochromic compounds were described as highly twisted molecules, with large dihedral angles ($\Phi > 25°$), packed within an open structure. Molecules appear to be quite isolated because of long intermolecular distances, as observed for instance in the model compound *N*-salicylidene 2-chloroaniline.[54] Some molecules such as *N*-salicylidene aniline present polymorphism and can crystallize in one thermochromic phase (β_1) as well as two photochromic phases (α_1 and α_2).[55,56] Interestingly, *N*-salicylidene aniline derivatives are only thermochromic in solution because of the low stability of the *trans*-keto form in this medium. Solid-state optical properties of *N*-salicylidene aniline derivatives are also influenced by the molecular environment, as shown by the incorporation of these molecules in polymethyl methacrylate,[48] MCM41 mesoporous silica,[57–59] liquid crystals,[60] organogelators and clathrates,[61–67] Na-Y zeolite[59,68] or micelles.[59] More recently, we have shown that the crystal structure was not the only factor to take into account to predict thermo- and photochromism of *N*-salicylidene anilines in the solid state.[42] Indeed, both electronic and structural aspects must be considered to properly predict optical properties. In this paper, we propose a new strategy to gain a better control of the crystal structure using crystal packing directing effect moieties. This possibility was thought after the analysis of the crystal structure of *N*-salicylidene 2-aminopyridine,[52,69,70] where an intramolecular H-bond between imine and pyridine ring locks the molecule in a planar geometry and gives a closed structure. Here, a rational crystal engineering approach is applied for the first time to the *N*-salicylidene aniline derivatives system. New N-heterocycle derivatives that are predesigned to lead to a controlled crystal structure with selected supramolecular interactions have been designed and synthesized. In the crystal network, *N*-salicylidene aniline derivatives are considered as nodes and supramolecular interactions (H-bonds, π–π stacking, CH–π and ionic interactions) as linkers. *N*-Salicylidene 4-amino-1,2,4-triazole (Hsaltrz) and *N*-salicylidene 5-aminotetrazole (Hsaltz) (Scheme 1a,b) present dense supramolecular networks based on intermolecular H-bonding interactions, although *N*-salicylidene 4-amino-3,5-bis(pyridine-2-yl)-1,2,4-triazole (Habs) and *N*-salicylidene (1,10)-phenanthrolin-5-amine (Hsalphen) (Scheme 1c,d) reveal mostly π–π stacking interactions. The potassium salt of *N*-salicylidene 5-aminotetrazolate (Ksaltz) (Scheme 1e) was studied to probe the impact of ionic interactions. All compounds are discussed as family members selected to lead to specific optical properties. From nonfunctional Hsaltrz, we could make either thermochromic molecules (Hsaltz and Ksaltz) by adding strong intermolecular H-bonds and ionic interactions or a photochromic molecule (Habs) by isolating the triazole moiety by two pyridine rings. Hsalphen is similar to Habs from a crystallographic point of view but however presents thermochromic properties. Optical properties of these compounds have been fully discussed in light of the supramolecular interactions revealed by the crystal structures. A complementary computational study carried out on isolated molecules and on molecules in the crystal packing strongly supports the optical properties of these materials.

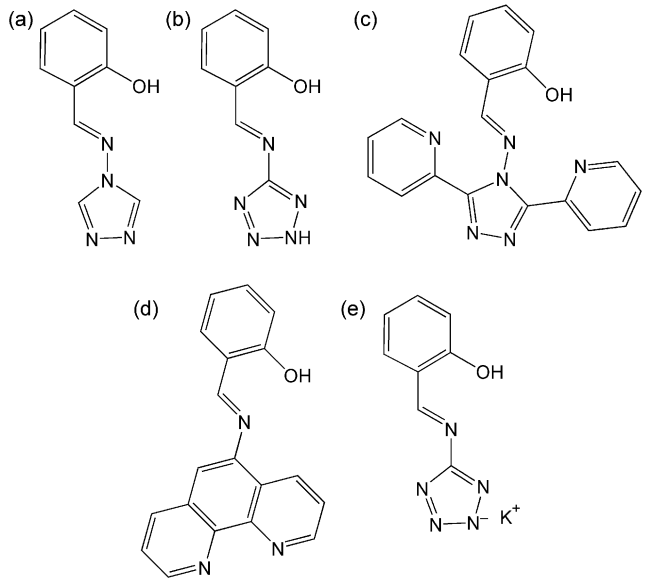

Scheme 1. Molecular scheme of Hsaltrz (a), Hsaltz (b), Habs (c), Hsalphen (d) and Ksaltz (e).

Results and Discussion

Syntheses and Crystallization

Purification of Hsaltz and Hsalphen was very difficult because the crude products systematically contained a large amount of unreacted salicylaldehyde in contrast to other *N*-salicylidene aniline derivatives. These impurities were successfully extracted by sonication in hexane and single crystals were obtained by slow evaporation of concentrated ethyl ether solutions. Slow sublimation of Habs at 110 °C under vacuum led to the growing of single crystals on the cold finger condenser of our sublimator setup. Single crystals of Hsaltrz were obtained by an unconventional method. For this experiment, we used the nucleophilicity of 4-amino-1,2,4-triazole, which can trap salicylaldehyde molecules, slowly released by the hydrolysis of a sodium salt of *N*-salicylidene *p*-aminobenzenesulfonate in methanol. A Cu^{II} salt, inserted in the reaction medium, is assumed to

ease the production of a pure white product of Hsaltrz, which slowly crystallizes (Scheme S1, Supporting Information).

Structural Aspects

Crystal Structure of N-Salicylidene 4-Amino-1,2,4-triazole (Hsaltrz)

Hsaltrz crystallizes in the monoclinic space group $P2_1/n$ (Table S1, Supporting Information). Two molecules in the enol form were distinguished in the asymmetric part of the unit cell (Figure 2). The bond lengths C^9–O^{14} and C^{109}–O^{114} of 1.351(2) and 1.350(2) Å respectively, confirm the presence of the enol form (Table 1, Scheme 2). In addition, the lengths of C^8–C^7 [1.458(2) Å] and C^{108}–C^{107} [1.456(6) Å] are in the range for single bonds, whereas the lengths for C^7–N^6 [1.279(2) Å] and C^{107}–N^{106} [1.279(2) Å] are in the range for double bonds[71] (Table 1). No bond length difference is noted between the two molecules of the asymmetric part of the unit cell. In contrast, a change in the dihedral angle between the aromatic rings is clearly distinguished [Φ_1 = 16(1)°, $\Phi_{1'}$ = 6(1)°, where Φ_1 and $\Phi_{1'}$ are measured on molecules 1 and 2, respectively] and is accompanied by different torsion angles $C^{(10)5}$–$N^{(10)4}$–$N^{(10)6}$–$C^{(10)7}$: Γ_1 = 15(1)° and $\Gamma_{1'}$ = 6(1)° (Table 1). The distances between H^2, H^{102} and the nearest H from the triazole ring are 2.15(2) Å and 2.19(2) Å (Table 1). According to some authors,[61] these differences can be interpreted as a slight change in the electronic conjugation of the molecule. Interestingly, Hsaltrz develops a new type of molecular geometry for the two molecules included in the asymmetric part of the unit cell where the intramolecular H-bond between the alcohol and imine functions is broken by rotation of the phenolic ring (Figure 2) and replaced by softer intramolecular H-bonds between the CH_{imine} and $O_{alcohol}$ atoms [C^7–H^7···O^{14} 2.38(2) Å and C^{107}–H^{107}···O^{114} 2.40(2) Å] (Table 2). Considering the loss of energy led by the absence of the usual intramolecular H-bond, the system has counterbalanced it by the formation of a strong intermolecular H-bond between a nitrogen atom of the triazole ring and the alcohol function [O^{14}–H^{14}···N^{102} 1.74(2) Å, O^{114}–H^{114}···N^1 1.76(2) Å] (Table 2 and Figure 2). The triazole ring has a strong structure-directing effect that drives molecules to leave their normal molecular geometry to allow the formation of strong intermolecular H-bonds. The packing is also highly modified because of the formation of supramolecular zigzag double chains (leading to a supramolecule; Figure 2). In each chain, a sequence of ···–Hsaltrz-2–Hsaltrz-1–Hsaltrz-2–Hsaltrz-1–··· is identified (Table 1 and

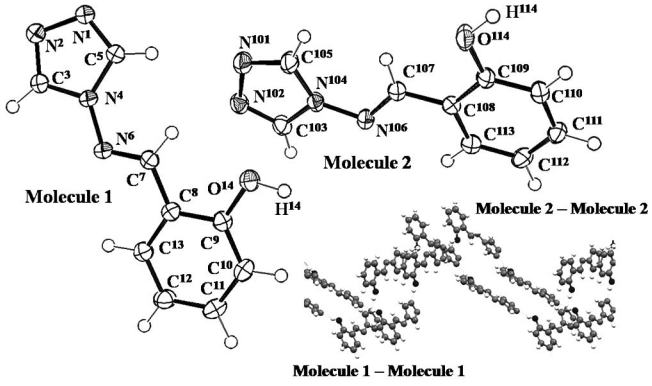

Figure 2. ORTEP view of the asymmetric part of the unit cell of Hsaltrz, showing 50% probability displacement ellipsoids. The inset shows the crystal packing involving intermolecular H-bonds (dotted line) and the formation of supramolecular double chains. The organization by pairs with (molecule 1/molecule 1) and (molecule 2/molecule 2) is clearly identified.

Table 1. Selected bond lengths [Å] and angles [°] for Hsaltrz, Habs, Hsalphen, Hsaltz and Ksaltz.

Compound	Hsaltrz	Habs	Hsalphen	Hsaltz	Ksaltz
Intermolecular distance [Å][a]	5.10	3.80	4.72	4.13	4.06
Φ_1 [°][b]	16 (1) 6 (1)	41 (1)	48 (1)	35 (1)	6 (1)
Φ_2 [°][c]	–	10 (1)	–	–	–
Φ_3 [°][d]	–	9 (1)	–	–	–
Γ [°][e]	15 (1) 6 (1)	62 (1)	45 (1)	33 (1)	1 (1)
C^4–O^5 [Å][f]	1.351 (2) 1.350 (2)	1.352 (2)	1.355 (3)	1.354 (3)	1.347 (5)
C^2–N^1 [Å][f]	1.279 (2) 1.279 (2)	1.279 (3)	1.283 (3)	1.293 (3)	1.283 (5)
C^2–C^3 [Å][f]	1.458 (2) 1.456 (6)	1.452 (3)	1.450 (3)	1.431 (4)	1.437 (6)
H^2···nearest H [Å][f]	2.15 (2) 2.19 (2)	–	2.39 (2)	–	–
N^0···H^2 [Å][f]	–	2.80 (3)	–	2.64(3)	2.49 (5)
K···N^2 [Å][g]	–	–	–	–	2.940 (3)
K···N^3 [Å][g]	–	–	–	–	2.806 (3)
K···$N^{3\#2}$ [Å][g]	–	–	–	–	3.170 (4)
K···N^4 [Å][g]	–	–	–	–	2.853 (4)
K···$N^{4\#2}$ [Å][g]	–	–	–	–	3.100 (4)
K···N^5 [Å][g]	–	–	–	–	2.886 (3)
K···$N^{5\#2}$ [Å][g]	–	–	–	–	2.869 (4)

[a] Distances between nearest molecular centroids. [b] Dihedral angle between phenolic plane and triazole (for Hsaltrz and Habs) or tetrazole (for Hsaltz and Ksaltz) or benzoic rings (for Hsalphen). [c] Dihedral angle between C^{15}–N^{16}–C^{17}–C^{18}–C^{19}–C^{20} pyridine ring and the triazole ring. [d] Dihedral angle between C^{21}–N^{22}–C^{23}–C^{24}–C^{25}–C^{26} pyridine ring and triazole ring. [e] Torsion angle centred on the imine function. [f] Distances with respect to Scheme 2. [g] Distances between K and the nearest nitrogen atoms.

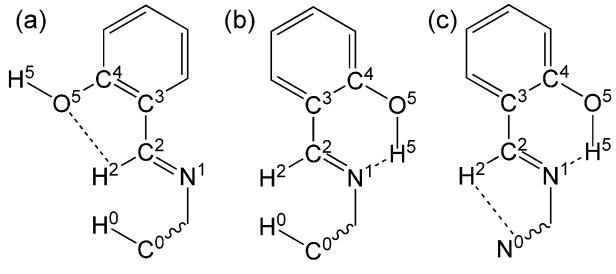

Scheme 2. Topology of the *N*-salicylidene moiety in Hsaltrz (a), Hsalphen (b) and in Habs and Hsaltz (c).

Table 2. Intramolecular and intermolecular H-bonds in Hsaltrz, Habs, Hsalphen, Hsaltz and Ksaltz.

	D–H···A	D–H [Å]	H···A [Å]	D···A [Å]	D–H···A [°]
Hsaltrz	O^{14}–H^{14}···$N^{102[a]}$	0.96 (2)	1.74 (2)	2.667 (2)	163 (2)
	O^{114}–H^{114}···$N^{1[b]}$	0.93 (2)	1.76 (2)	2.685 (2)	174 (2)
	C^{7}–H^{7}···O^{14}	0.97 (2)	2.38 (2)	2.736 (3)	101 (2)
	C^{107}–H^{107}···O^{114}	0.96 (2)	2.40 (2)	2.743 (2)	100 (1)
	C^{111}–H^{111}···$O^{114[c]}$	0.96 (2)	2.45 (2)	3.244 (2)	140 (2)
Habs	O^{14}–H^{14}···N^{6}	0.89 (2)	1.95 (3)	2.682 (2)	138 (2)
	O^{14}–H^{14}···N^{16}	0.89 (2)	2.36 (3)	3.098 (3)	140 (2)
	C^{7}–H^{7}···$N^{22[d]}$	0.97 (3)	2.45 (3)	3.400 (3)	167 (2)
	C^{26}–H^{26}···$N^{2[e]}$	1.00 (3)	2.60 (3)	3.333 (3)	131 (2)
Hsalphen	O^{23}–H^{23}···N^{15}	0.97 (3)	1.80 (3)	2.650 (3)	146 (2)
	C^{6}–H^{6}···$N^{1[f]}$	1.00 (3)	2.51 (3)	3.352 (3)	141 (2)
	C^{16}–H^{16}···$N^{1[g]}$	1.02 (3)	2.46 (2)	3.401 (3)	152 (2)
Hsaltz	O^{14}–H^{14}···N^{6}	0.94 (3)	1.75 (3)	2.602 (3)	151 (3)
	N^{4}–H^{4}···$N^{1[h]}$	0.92 (3)	1.90 (3)	2.805 (3)	167 (3)
Ksaltz	O^{1}–H^{1}···N^{1}	0.96 (5)	1.76 (5)	2.615 (4)	147 (5)
	C^{8}–H^{8}···N^{2}	0.93	2.49	2.837 (6)	102

[a] Symmetry operations: $x - 1, y, z$. [b] $x - 3/2, -y + 1/2, z + 1/2$. [c] $x - 1/2, 1/2 - y, 1/2 + z$. [d] $x + 1, y, z$. [e] $1 - x, 2 - y, -z$. [f] $1/2 - x, 1/2 + y, z$. [g] $-x, 2 - y, 1 - z$. [h] $x, 1 + y, z$.

Table 3. Intermolecular π–π stacking and C–H···π interactions in Hsaltrz, Habs, Hsalphen, Hsaltz and Ksaltz.

	Moiety 1	Moiety 2	Distance between centroids [Å]	Angle between moieties [°]
Hsaltrz	C^{8}–C^{7}–N^{6}–N^{4}	N^{1}–N^{2}–C^{3}–N^{4}–C^{5}	3.782 (2)	12 (1)
	C^{108}–C^{107}–N^{106}–N^{104}	N^{101}–N^{102}–C^{103}–N^{104}–C^{105}	3.552 (2)	6 (1)
	C^{8}–C^{7}–N^{6}–N^{4}	C^{8}–C^{9}–C^{10}–C^{11}–C^{12}–C^{13}	3.934 (2)	4 (1)
	C^{108}–C^{107}–N^{106}–N^{104}	C^{108}–C^{109}–C^{110}–C^{111}–C^{112}–C^{113}	3.481 (2)	12 (1)
	C^{108}–C^{109}–C^{110}–C^{111}–C^{112}–C^{113}	C^{105}–H^{105}	2.87 (2)	3 (1)
Habs	C^{15}–N^{16}–C^{17}–C^{18}–C^{19}–C^{20}	C^{15}–N^{16}–C^{17}–C^{18}–C^{19}–C^{20}	3.805 (2)	0 (1)
	C^{21}–N^{22}–C^{23}–C^{24}–C^{25}–C^{26}	C^{15}–N^{16}–C^{17}–C^{18}–C^{19}–C^{20}	3.805 (2)	0 (1)
	N^{1}–N^{2}–C^{3}–N^{4}–C^{5}	N^{1}–N^{2}–C^{3}–N^{4}–C^{5}	3.805 (2)	0 (1)
	C^{8}–C^{9}–C^{10}–C^{11}–C^{12}–C^{13}	C^{8}–C^{9}–C^{10}–C^{11}–C^{12}–C^{13}	3.805 (2)	0 (1)
	C^{7}–C^{8}–N^{4}–N^{6}	C^{7}–C^{8}–N^{4}–N^{6}	3.805 (2)	0 (1)
Hsalphen	C^{5}–C^{6}–C^{11}–C^{12}–C^{13}–C^{14}	C^{5}–C^{6}–C^{11}–C^{12}–C^{13}–C^{14}	3.603 (2)	0 (1)
	N^{1}–C^{2}–C^{3}–C^{4}–C^{12}–C^{13}	C^{5}–C^{6}–C^{11}–C^{12}–C^{13}–C^{14}	3.985 (2)	2 (1)
	N^{1}–C^{2}–C^{3}–C^{4}–C^{12}–C^{13}	N^{10}–C^{9}–C^{8}–C^{7}–C^{14}–C^{11}	4.228 (2)	1 (1)
	N^{1}–C^{2}–C^{3}–C^{4}–C^{12}–C^{13}	C^{17}–C^{18}–C^{19}–C^{20}–C^{21}–C^{22}	4.239 (2)	6 (1)
	C^{5}–N^{15}–C^{16}–C^{17}	N^{1}–C^{2}–C^{3}–C^{4}–C^{12}–C^{13}	3.713 (2)	8 (1)
	N^{10}–C^{9}–C^{8}–C^{7}–C^{14}–C^{11}	C^{2}–H^{2}	2.86 (3)	3 (1)
Hsaltz	N^{1}–N^{2}–N^{3}–N^{4}–C^{5}	N^{1}–N^{2}–N^{3}–N^{4}–C^{5}	3.468 (2)	0 (1)
Ksaltz	C^{9}–N^{1}–C^{8}–C^{7}	C^{7}–C^{3}–C^{2}–C^{4}–C^{5}–C^{6}	3.694 (2)	5 (1)
	C^{9}–N^{1}–C^{8}–C^{7}	N^{5}–N^{4}–N^{3}–C^{9}–N^{2}	3.504 (2)	2 (1)

Figure 2). The double chain architecture is not only stabilized by H-bonds but also by π–π stacking interactions (Figure 2) between the imine function of a molecule of a chain and salicyl or a triazole ring of a molecule of the other chain (Table 3). In contrast, double chains are almost isolated from each other. Only a weak intermolecular H-bond between the alcohol function of a molecule of one chain and a CH from the salicyl ring of a molecule of another chain [C^{111}–H^{111}···O^{114} 2.45(2) Å] is found (Table 2). A weak CH–π interaction between a salicyl ring of a molecule in a chain and a CH of a triazole ring of the nearest chain [C^{108}–C^{109}–C^{110}–C^{111}–C^{112}–C^{113}···H^{105}–C^{105} 2.87(2) Å] is also noted (Table 3).

Crystal Structure of N-Salicylidene 4-Amino-3,5-bis(pyridine-2-yl)-1,2,4-triazole (Habs)

Habs crystallizes in the triclinic space group $P\bar{1}$ (Table S1, Supporting Information). The asymmetric part of the unit cell contains one molecule in the enol form (Figure 3). It is possible to clearly identify it: the C^{9}–O^{14} [1.352(2) Å] and C^{8}–C^{7} [1.452(3) Å] bond lengths are characteristic of single bonds and the N^{6}–C^{7} [1.279(3) Å] bond length reveals a double bond[71] (Table 1). Small dihedral angles are observed between the triazole and pyridine rings [Φ_2 = 10(1)° between C^{15}–N^{16}–C^{17}–C^{18}–C^{19}–C^{20} pyridine and the triazole ring and Φ_3 = 9(1)° between C^{21}–N^{22}–C^{23}–

C^{24}–C^{25}–C^{26} pyridine and triazole ring] (Table 1). In contrast, a large dihedral angle is identified between the salicyl and the triazole rings [Φ_1 = 41(1)°] (Table 1). In addition, the imine function is observed to be away from the "pyridine-triazole-pyridine" plane [N^{22}···H^7 2.80(3) Å]. The torsion angle C^3–N^4–N^6–C^7 (Γ) is equal to 62(1)° (Table 1). A strong intramolecular H-bond exists between the alcohol and imine functions, as commonly identified in *N*-salicylidene aniline derivatives [O^{14}–H^{14}···N^6 1.95(3) Å] (Figure 3 and Table 2).[51] Another soft intramolecular H-bond is also observed between the alcohol function and the nearest nitrogen of one pyridine ring [O^{14}–H^{14}···N^{16} 2.36(3) Å]. Finally, two weak intermolecular H-bonds are observed between the imine group and a pyridine ring of the nearest molecule [C^7–H^7···N^{22} 2.45(3) Å] and between triazole and the pyridine ring of another molecule [C^{26}–H^{26}···N^2 2.60(3) Å] (Figure 3 and Table 2). These interactions explain the position of the nitrogen of the pyridine rings in the molecule. Crystal packing is very compact because of short intermolecular distances ($d_{\text{centroid–centroid}}$ = 3.80 Å) (Table 1). Strong π–π stacking interactions are noted between all aromatic rings of one molecule and the same rings in nearest symmetric molecules (Figure 3 and Table 3). In contrast to Hsaltrz, no CH–π interaction is observed.

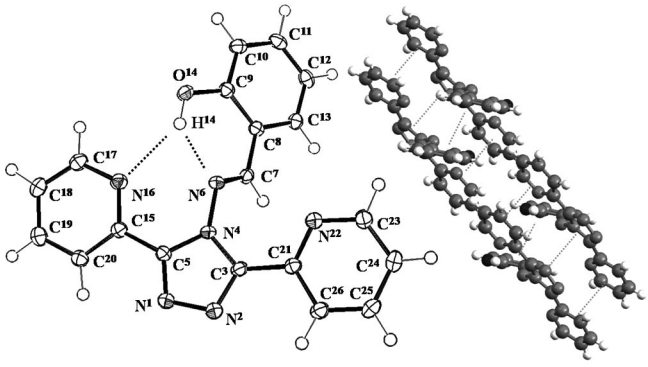

Figure 3. ORTEP view of the asymmetric part of the unit cell of Habs, showing 50% probability displacement ellipsoids. Intramolecular bifurcated H-bonds are indicated as dotted lines. View along the *b* axis of the crystal packing showing extended intermolecular π–π stacking interactions (indicated as dotted lines).

Crystal Structure of N-Salicylidene 5-Amino-1,10-phenanthroline (Hsalphen)

Hsalphen crystallizes in the orthorhombic space group *Pbca* (Table S1, Supporting Information). As in Habs, one molecule in the enol form is observed in the asymmetric part of the unit cell (Figure 4). The C^{22}–O^{23} [1.355(3) Å] and C^{16}–C^{17} [1.450(3) Å] bond lengths indicate single bonds and C^{16}–N^{15} [1.283(3) Å] reveals a double bond[71] (Table 1). Two planes are present in the molecule: the first one is formed by the salicyl ring and the imine function, which are coplanar, and the second one is created by the phenanthroline moiety, which is perfectly planar. A large dihedral angle Φ_1 = 48(1)° and a large torsion angle (C^6–N^5–N^{15}–C^{16}) Γ_1 = 45(1)° are noted between them (Table 1). The distance between H^{16} and H^6 is found as 2.39(2) Å (Table 1). A strong intramolecular H-bond [O^{23}–H^{23}···N^{15} 1.80(3) Å] is observed between the alcohol and imine functions as in Habs (Figure 4 and Table 2). Although the dihedral angle with the salicyl ring is similar in Habs and Hsalphen, the distance between H^{23} and N^{15} is significantly shorter [1.80(3) Å] in Hsalphen in comparison to the distance between H^{14} and N^6 in Habs [1.95(3) Å] (Table 2). This observation constitutes another proof of the absence of a link between Φ and the intramolecular H-bond strength.[42] Crystal packing of Hsalphen is directed by the formation of strong intermolecular π–π stacking interactions between phenanthroline moieties, imine functions and salicyl rings (phen···phen 3.90 Å between centroids; $d_{\text{between molecular centroids}}$ = 4.72 Å) (Table 1 and Figure 4). In addition, two weak intermolecular H-bonds [C^6–H^6···N^1 2.51(3) Å and C^{16}–H^{16}···N^1 2.46(2) Å] (Table 3) and a CH···π interaction between phenanthroline moieties (C^2–H^2···N^{10}–C^{11}–C^{14}–C^7–C^8–C^9) complete such a dense supramolecular network (Table 3).

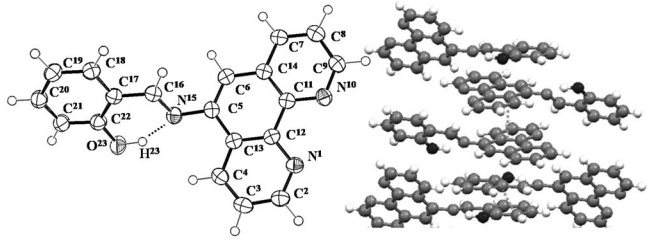

Figure 4. ORTEP view of the asymmetric part of the unit cell of Hsalphen, showing 50% probability displacement ellipsoids. Intramolecular H-bond is indicated as a dotted line. View along the *b* axis of the crystal packing showing intermolecular π–π stacking interactions (indicated as dotted lines).

Crystal Structure of N-Salicylidene 5-Aminotetrazole (Hsaltz)

Hsaltz crystallizes in the monoclinic space group *C*2/*c* (Table S1, Supporting Information). In the asymmetric part of the unit cell, one highly twisted molecule in the enol form is observed (Figure 5). The C^9–O^{14} [1.354(3) Å] and C^7–C^8 [1.431(4) Å] bond lengths indicate single bonds and C^7–N^6 [1.293(3) Å] reveals a double bond[71] (Table 1). The molecule is characterized by a large dihedral angle [Φ_1 = 35(1)°], a large torsion angle N^1–C^5–N^6–C^7 Γ_1 = 33(1)° and a strong intramolecular H-bond [O^{14}–H^{14}···N^6 1.75(3) Å] between the imine and alcohol functions (Tables 2 and 3, Figure 5), which is clearly stronger than in Hsalphen and Habs. Crystal packing is directed, as in Hsaltrz, by the formation of an intermolecular H-bond between the proton of the tetrazole moiety and the nearest tetrazole ring [N^4–H^4···N^1 1.90(3) Å] (Figure 5 and Table 2). The distance between molecular centroids is evaluated as 4.13 Å and the distance between N^1 and H^7 was found as 2.64(3) Å (Table 1). Intermolecular H-bonds lead to a supramolecular network where supramolecular double chains (supramolecules) are clearly distinguished (Figure 5). Cohesion between these two chains originates from intermolecular π–π stacking in-

teractions between the tetrazole moieties (tz···tz 3.47 Å between centroids) (Figure 5 and Table 3). No CH–π interaction is observed.

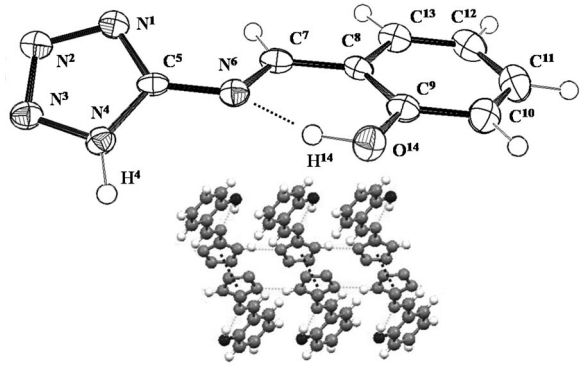

Figure 5. ORTEP view of the asymmetric part of the unit cell of Hsaltz, showing 50% probability displacement ellipsoids. Intramolecular H-bond is indicated as a dotted line. View of the crystal packing showing the formation of supramolecular double chains built with intermolecular π–π stacking interactions (indicated as dotted lines) and with intermolecular H-bonds (indicated as dotted lines).

Crystal Structure of the Potassium Salt of N-Salicylidene 5-Aminotetrazolate (Ksaltz)

Ksaltz also crystallizes in the monoclinic space group *C*2/*c* (Table S1, Supporting Information). However, it is not isostructural to Hsaltz. An almost planar molecule is observed in the asymmetric part of the cell. A small dihedral angle between the aromatic rings (Φ_1) of 6(1)° was measured (Figure 6 and Table 1), which is clearly lower than that in the Hsaltz structure [35(1)°]. The molecule is in the fundamental enol form (Figure 6). The C^2–O^1 and C^7–C^8 bond lengths [1.347(5) and 1.437(6) Å] are typical of single bonds and C^8–N^1 [1.283(5) Å] of a double bond[71] (Table 1). Two intramolecular H-bonds are noted in Ksaltz.

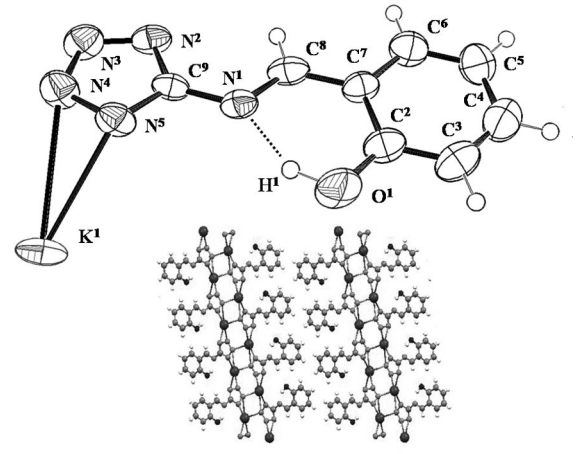

Figure 6. ORTEP view of the asymmetric part of the unit cell of Ksaltz, showing 50% probability displacement ellipsoids. Intramolecular H-bond is indicated as a dotted line. View of the crystal packing, along the *b* axis, showing a planar arrangement of ionic planes containing potassium and tetrazolate ions and organic planes containing others functions.

A strong H-bond is present between the alcohol and the imine functions [$O^1H^1\cdots N^1$ 1.76(5) Å], which is highly similar to the intramolecular H-bond observed in Hsaltz. A soft intramolecular H-bond is also observed between a nitrogen of the tetrazolate ring and the hydrogen of the imine function (C^8–$H^8\cdots N^2$ 2.49 Å), which was not present in Hsaltz because of the large dihedral angle. Crystal packing is clearly directed by ionic interactions between potassium and tetrazolate ions. The structure is packed in planes: a stack of ionic planes and organic planes with salicyl and imine moieties as observed in Figure 6. Potassium ions are present within disorganized atomic spheres and no clear geometric environment can be derived (Table 1). The closed packing is not only stabilized by ionic interactions but also by strong π–π stacking interactions between the imine group and the salicyl ring [$d_{\text{inter planes}}$ = 3.694(2) Å] and between the imine group and the tetrazolate ring [$d_{\text{inter planes}}$ = 3.504(2) Å].

Optical Properties

Thermochromic and Photochromic Phenomena

As shown in Figure 7, Hsaltrz and Habs remain white over the whole investigated temperature range (298–77 K). In contrast, Hsalphen, Hsaltz and Ksaltz exhibit moderate to strong thermochromism upon cooling to 77 K. Hsalphen has a yellow/orange coloration that evolves from dark to light orange when the temperature is decreased. Hsaltz is only slightly thermosensitive. Its colour varies from very pale yellow at room temperature to white at liquid-nitrogen temperature. In contrast, Ksaltz clearly changes its colour: the sample is yellow at room temperature and turns to white at low temperature. Colour difference between Hsaltz and Ksaltz is clearly distinguished by naked eyes at room temperature.

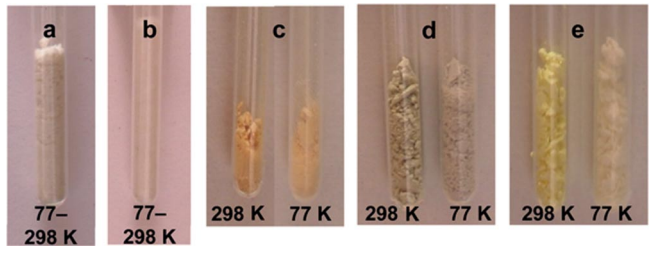

Figure 7. Photograph of powders of Hsaltrz (a) and Habs (b) over the temperature range 298–77 K and of Hsalphen (c), Hsaltz (d) and Ksaltz (e) at 298 and 77 K. Thermochromism is identified for c, d (very weak) and e (strong).

All compounds were analyzed by diffuse reflectance spectroscopy as pure solid powder samples[72] to avoid matrix and environment effects that are known to intensively modify the optical properties of *N*-salicylidene aniline derivatives.[48,58–68] Figure 8a shows the Kubelka Munk spectra of Hsaltrz, Hsaltz and Ksaltz. A bathochromic shift is observed from Hsaltrz to Hsaltz and Ksaltz. Hsaltrz only

absorbs in the UV range (below 400 nm). This absorption is typical of the enol form, which is largely predominant as described in the crystallographic section. In Hsaltz, the enol band is shifted by approximately 18 nm to lower energies (an intense band is noted at approximately 430 nm), which leads to the slightly yellow coloration of the product. No band from the keto forms is observed. The intense band in the UV range of the spectrum (at approximately 430 nm) is attributed to the enol form. The colour difference between Hsaltz and Ksaltz is ascribed to the presence of a band with a maximum in the visible range of the spectrum at approximately 460 nm for Ksaltz. This band is typical of the *cis*-keto form of the molecule. Hsaltrz, Hsaltz and Ksaltz are observed to be nonphotochromic at room temperature. Indeed, irradiation at 254 nm for 1 h does not lead to modification of the Kubelka Munk spectra.

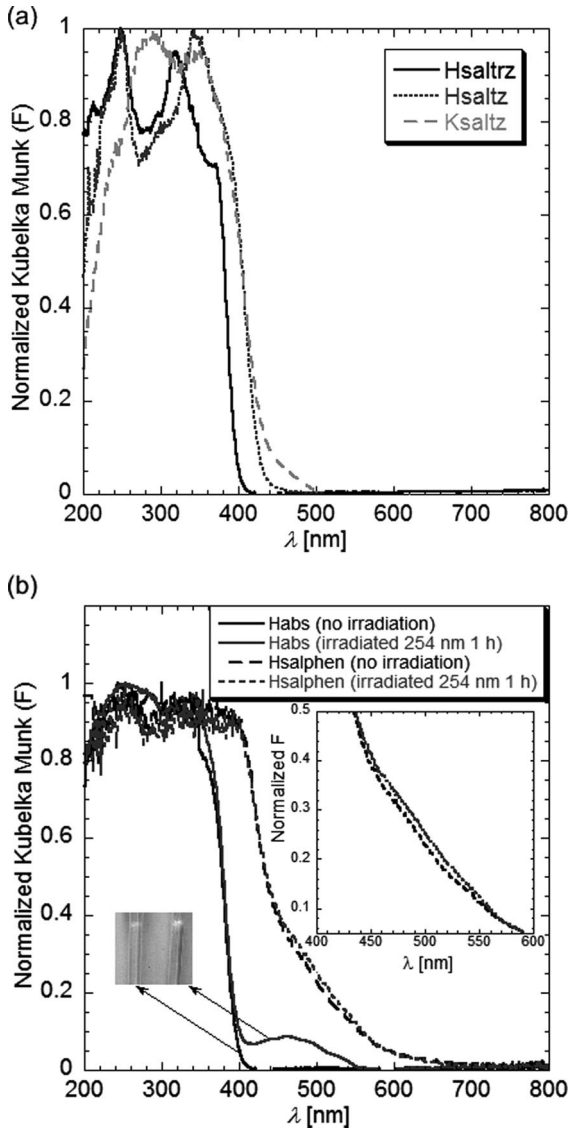

Figure 8. Kubelka Munk spectra at 298 K of Hsaltrz, Hsaltz and Ksaltz (a) and of Habs and Hsalphen before and after UV irradiation (b). Photochromism is clearly identified for Habs. The inset in Figure 8b reveals weak photochromism for Hsalphen at 298 K.

Figure 8b shows the Kubelka Munk spectra of Habs and Hsalphen. Habs presents an intense band in the UV range, a feature that fits with the white colour of the compound. Irradiation of the sample at 254 nm during 1 h leads to a clear spectral change in the visible range. A new maximum is noted at 465 nm and is attributed to the formation of a photoinduced metastable form: the *trans*-keto isomer.[42] The absence of the *cis*-keto form is assumed for this compound. For Hsalphen, a nonresolved intense band in the UV range of the spectrum is noted with a bathochromic shift of approximately 50 nm. A second broad band is observed in the visible (maximum unresolved at approximately 450 nm) and is attributed to the *cis*-keto form. Irradiation at 254 nm for 1 h leads to a very slight change in the Kubelka Munk function intensity around 500 nm, which is attributed to the formation of the *trans*-keto isomer. The increase in the *trans*-keto band is less intense in Hsalphen than in Habs but is still detected with the naked eye.

Thanks to the clear spectral change under UV irradiation of Habs, a study of the thermal relaxation of the system in the *trans*-keto form was conducted by using time dependant diffuse reflectance spectroscopy. Figure 9 shows the evolution of the Kubelka Munk function at 465 nm, which is near the band maximum of the *trans*-keto form (Figure 8b). Irradiation at 254 nm for 20 min induces a large increase in F. After stopping the irradiation, leading to rapid thermal relaxation, complete recovery of the initial value in approximately 4 h is observed. This cycle is fully reproducible, as shown in Figure 9. The relaxation appears to be elaborated and contains more than one chemical relaxation pathway. Attempts to fit this curve with an exponential function failed. The photoisomerization process is also photochemically reversible, as shown in Figure 10. After photoexcitation at 254 nm and thermal relaxation over 10 min, illumination at 450 nm induces a fast return to the initial F value (Figure 10). Afterwards, an unexpected "spring-type" effect is observed without further stimulus. Over a few minutes, the signal increased to approximately 20% of the maximum value reached. The system reacts spontaneously to the energy flow induced by the second irradiation by

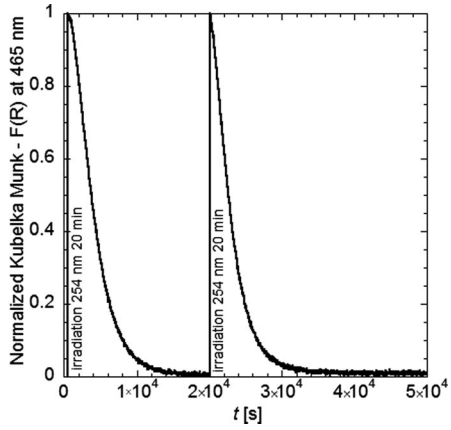

Figure 9. Time dependence of the Kubelka Munk function (F) of Habs at 465 nm, showing the reproducible thermal relaxation of the metastable *trans*-keto form.

trying to return to the metastable state. After this abnormal increase, a subsequent thermal relaxation of the *trans*-keto form is observed.

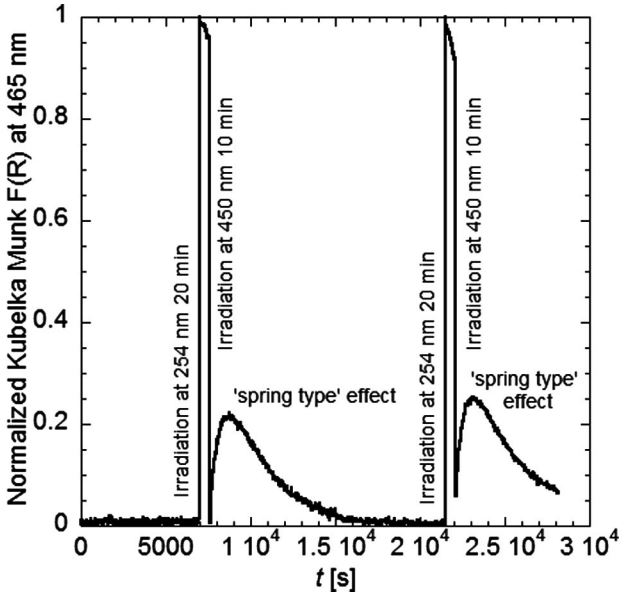

Figure 10. Time dependence of the Kubelka Munk function (F) of Habs at 465 nm, showing the reproducible photochemical relaxation of the metastable *trans*-keto form leading to an unexpected "spring-type" effect.

Emission Spectroscopy

Fluorimetry was used to study energy levels involved during the thermo- and photoinduced processes. Analyses were conducted on pure solid powder samples. Figure 11a shows the emission spectra at 400 nm of Hsaltz and Ksaltz. One intense emission is observed, centred at 536 nm for Hsaltz and at 540 nm for Ksaltz, which is assigned to the emission of the excited *cis*-keto* form (Table S2, Supporting Information). Thus, the two compounds seem to have very similar emission properties. Figure 11b presents the emission spectra of Hsaltrz and Hsalphen at 350 nm, which are clearly different. More than one contribution is noted. A first intense emission band, centred at 523 nm and 569 nm for Hsaltrz and Hsalphen, respectively, is attributed to the radiative relaxation of the excited *cis*-keto* form (Table S2, Supporting Information). Thus, a shift of this band is clearly noted between Hsaltrz and Hsalphen. A second band is observed in both spectra at very narrow wavelengths, 441 and 438 nm for Hsaltrz and Hsalphen, respectively (Table S2, Supporting Information). This emission is attributed to the radiative relaxation of the excited enol* form. Finally, it is important to notice that a third emission contribution is only observed in Hsalphen, centred at 420 nm, which is believed to be a radiative relaxation of an enol form in a more relaxed conformation (Table S2, Supporting Information). Figure 11c represents the emission spectrum of Habs at 400 nm. The main emission band noted at 544 nm is attributed to the excited *cis*-keto* radiative relaxation. A second major contribution is observed at 476 nm (Table S2, Supporting Information). This less-intense band could originate from three excited molecules: the enol form, a more relaxed *cis*-keto form or the molecule in an intermediate state as described in the next section. Unfortunately, we are not able to distinguish between these three molecules because of the proximity or the superposition of some absorption bands. It is important to notice that in all spectra (Hsaltrz, Habs, Hsalphen, Hsaltz and Ksaltz), a low emission is observed at approximately 650 nm that cannot be assigned with confidence. The origin of this emission can be the radiative de-excitation of either an excited *cis*-keto form higher in energy than the previous one or the excited *trans*-keto* form.

Photoisomerization Model in Single Crystals

In order to gain a better understanding of factors that control the intriguing optical properties of Hsalphen and Habs, we have investigated their photoisomerization by computational means (see Experimental Section). Firstly, we have examined the enol, *cis*-keto and *trans*-keto equilibria for isolated Hsalphen and Habs molecules in the ground state (GS) and in the first singlet (S^1) and the first triplet (T^1) excited states. Table S3 (Supporting Information) re-

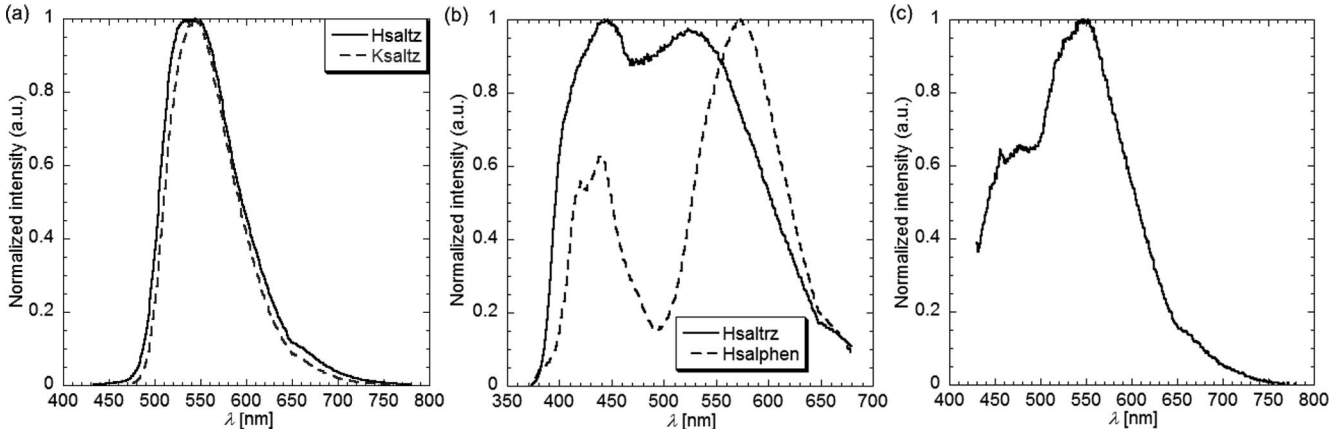

Figure 11. Solid-state emission spectra at 298 K of (a) Hsaltz and Ksaltz at 400 nm (b) Hsaltrz and Hsalphen at 350 nm and of (c) Habs at 400 nm.

ports the computed relative energy of the different species and the activation barrier for *cis*-keto/*trans*-keto isomerization in the respective states. The energy profiles for this latter step are depicted in Figure 12.

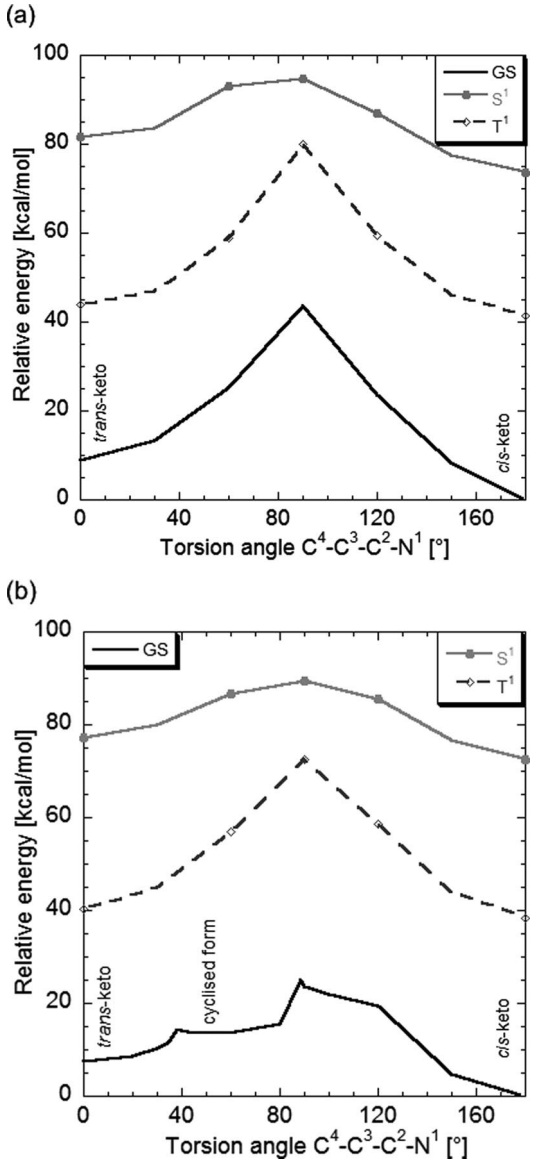

Figure 12. Calculated energy evolution for the ground state (GS) and for the first singlet (S^1) and first triplet excited states (T^1) during the photoisomerization of (a) Hsalphen and (b) Habs. The torsion angle C^4–C^3–C^2–N^1 is given relative to Scheme 2.

These results reveal that, in both cases, the proton transfer step (enol to *cis*-keto) is energetically disfavoured in the ground state and favoured in the first singlet and first triplet excited states.[73] Interestingly, the proton transfer in the GS for Habs is significantly more endothermic (11.3 kcal/mol) than for Hsalphen (7.6 kcal/mol) or for previously studied aminopyridines derivatives (7–9 kcal/mol).[42] This could account for the absence of thermochromism in Habs, whereas all the other considered molecules, except Hsaltrz, show thermochromism.

The computed activation barrier for *cis*-keto to *trans*-keto isomerization indicates that, for both molecules, photoisomerization must take place through the S^1 state as previously reported (Table S3, Supporting Information; Figure 12).[42] For Hsalphen, the activation barrier in the S^1 state (21.0 kcal/mol) nicely corresponds to those of *N*-salicylidene aminopyridine derivatives (20–21 kcal/mol),[42] whereas in the case of Habs it is much lower (16.9 kcal/mol). This result supports the observation of photochromism for these molecules.

It is interesting to note that the energy profile for photoisomerization of Habs in the ground state unexpectedly reveals the presence of an intermediate in the pathway to the *trans*-keto form (Figures 12 and 13). Formation of a cyclized intermediate can be accounted for by the developing zwitterionic character of Habs (heterolytic breaking of the C^7–C^8 double bond) with rotation (see Table S5, Supporting Information, for charges). Indeed, the presence of a nucleophilic nitrogen atom (N^{22}) in this case allows addition of this latter onto the developing positive charge on C^7, which is rapidly followed by addition of the phenolic oxygen (O^{14}) onto the pyridine ring (C^{23}) to form a six-membered ring (Figure 13b). This cyclized intermediate can then lead to the *trans*-keto form through a very low activation

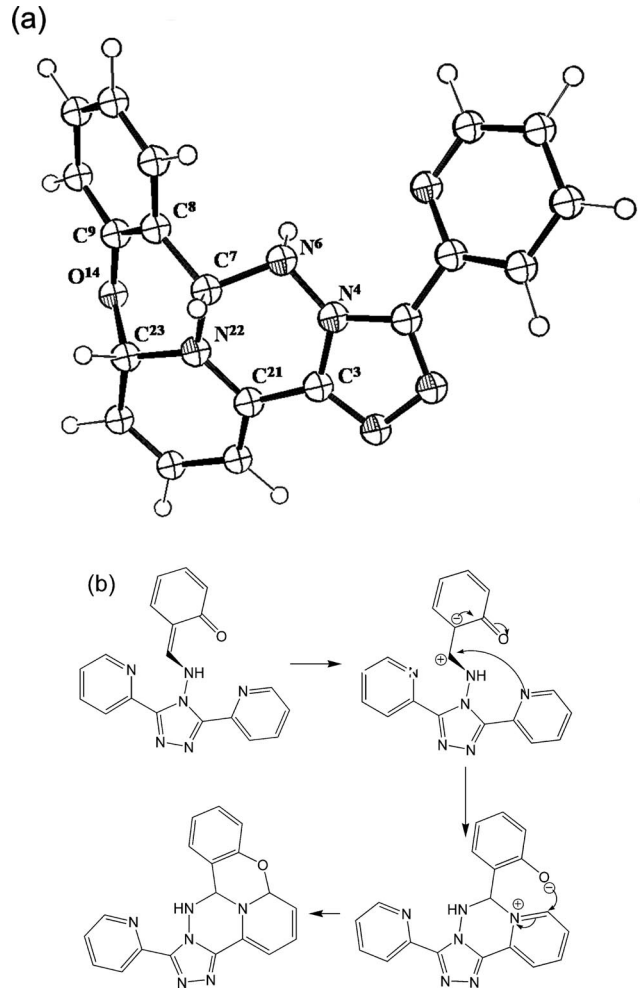

Figure 13. (a) Optimized structure of the cyclized form of Habs. (b) Suggested mechanism for the formation of the cyclized form involving a zwitterionic form of Habs.

barrier (0.1 kcal/mol), which suggests that the equilibrium between these two forms must be thermally accessible. The influence of this new cyclized form on the experimental results will be discussed in the next section. Note that, even if this mechanism allows a low activation barrier in the GS (lower than that for Hsalphen or aminopyridine derivatives[42]), no thermochromism upon heating is observed for this compound (≈100 °C).

Because of the expected importance of crystal packing on the photochromic properties of Habs and Hsalphen, we also investigated, by computational means, the *cis*-keto/*trans*-keto isomerization by taking in account a model of the crystal packing obtained by single-crystal X-ray diffraction analyses (Figures 3 and 4). The influence of crystal packing on the photoisomerization was probed by estimating the relative stabilization induced by placing the different species in their crystal (see Experimental Section).[74] Obtained stabilization energies (from 0 to 7.2 kcal/mol) indicate that although the packing is closed, due to the strong π–π stacking network, it does not prevent isomerization. Analysis of the transition-state structure shows that, as previously observed for *N*-salicylidene aminopyridine derivatives, the preferred mechanism for isomerization resembles the pedal motion of a bicycle.[42] In both cases (although to a larger extent for Hsalphen), the TS structure is better stabilized by crystal packing than for the *cis*-keto form. This means that crystal packing should lead to an activation of the isomerization, which is in good agreement with the observed photochromism at room temperature.

Discussion

Novel, nitrogen-rich *N*-salicylidene aniline derivatives have been synthesized. Each molecule has been selected to promote a given supramolecular interaction (intra- or intermolecular H-bonds, π–π stacking, ionic interaction) that allows their optical properties to be tuned.

Hsaltrz is distinguished from other *N*-salicylidene aniline derivatives thanks to a novel molecular geometry. Complete rotation of the salicyl ring leads to breakage of the intramolecular H-bond between the OH and N_{imine} moieties and allows the formation of supramolecular double chains with π–π stacking interactions. Thus, a crystal-directing effect of the electron-rich triazole ring is effective. This feature associated with phenolic ring rotation leads to a large change in the optical properties because the prototropic phenomenon is no longer thermally accessible. Photochromism at room temperature is also quenched because the molecular geometry and packing do not allow the photoisomerization to proceed.

Habs could be seen as a derivative of Hsaltrz, where the triazole ring is isolated thanks to two pyridine rings. The intermolecular H-bond between the triazole rings in Hsaltrz is no longer possible and thus no rotation of the salicyl ring is observed. However, the presence of triazole and pyridine rings linked to each other leads to a close molecular packing directed by the formation of strong π–π stacking interactions. Interestingly, the close crystal packing made with highly planar molecules is not sufficient to properly predict the optical properties of Habs, because, despite the fact it is expected to be thermochromic following the classification of Ogawa,[35,51] it is exclusively photochromic. This intriguing situation was recently met in the case of *N*-salicylidene aminopyridines.[42] Our calculations suggest that this unexpected absence of thermochromism associated with an absence of coloration of the compound in the whole studied temperature range (77–400 K), which is observed for the first time for this class of molecules, could be due to a higher reaction energy (more endothermic) for proton transfer in the ground state. On the other hand, in the first singlet excited state, the proton transfer is found to be exothermic, as for other studied derivatives, and the barrier to *cis*-keto/*trans*-keto isomerization is consistent with the observed photochromism at room temperature.

Kinetic study of the thermal relaxation of the photoinduced metastable *trans*-keto form indicates that the relaxation pathway is very complex. Our computational calculations have revealed the presence of a cyclized intermediate on the energy profile of Habs (Figure 12). This intermediate is predicted to be in equilibrium with the *trans*-keto form through a very low activation barrier. This new molecular scheme allows a rationalization of the complex thermal relaxation kinetics and in particular the unprecedented "spring-type" effect observed during the photochemical reversibility study to be proposed (Figure 10). Figure 14 suggests a schematic evolution of the population of the enol, the cyclized and the *trans*-keto forms during each step observed in Figure 9. We assume that the irradiation at 254 nm (step 1) leads to a large increase in the *trans*-keto form population and the formation of a small amount of the cyclized form. During the first minutes of the relaxation (step 2), the cyclized form rapidly relaxes to the *trans*-keto form. The input of the *trans*-keto form into the system slightly compensates for the thermal relaxation of this form to the enol form and then modifies the shape of the thermal relaxation from a normal exponential to a curve as observed in Figure 9. Finally, during the last step (step 3), normal kinetic relaxation from the *trans*-keto to the enol form is observed. The unexpected "spring-type" effect can also be thought by a similar reasoning (Figure 14b). Although steps 1 and 2 are the same as those described in Figure 14a, irradiation at 450 nm (step 3) leads to a zeroing of the *trans*-keto form population, but we assume that a significant population of the cyclized form remains present. A small amount of *trans*-keto form could be then reformed by relaxation of the cyclized form after a few minutes without any external stimulus (step 4), as observed in the experimental data (Figure 10, "spring-type" effect). Finally, the *trans*-keto form population then relaxes to the enol form to return to the initial situation (step 5).

Hsaltz is closely related to Hsaltrz. The tetrazolate ring is indeed more electron rich than a triazole ring, but it contains an N–H moiety that has an important crystal packing directing effect. Indeed, crystal packing is directed by the formation of an intermolecular H-bond between the tetra-

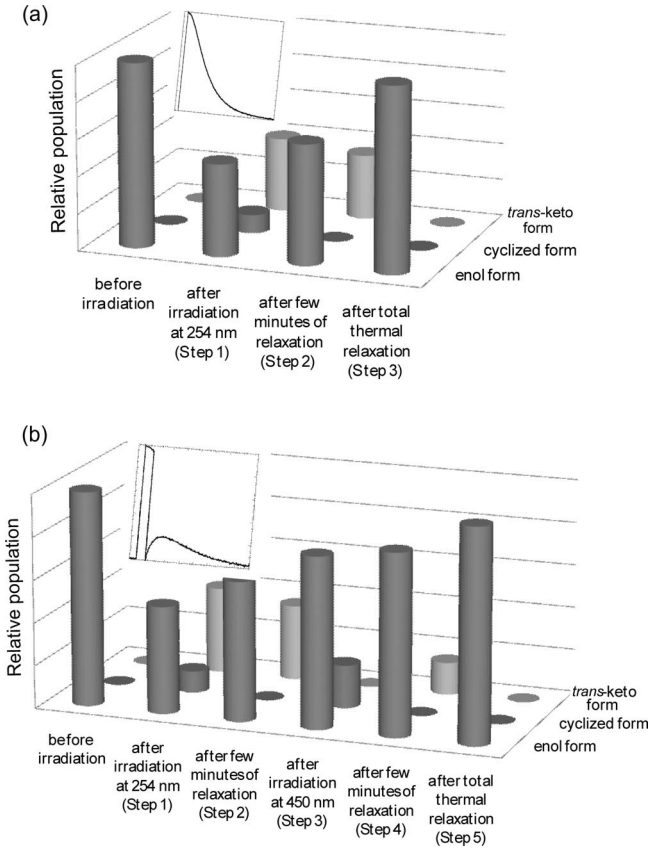

Figure 14. Suggested evolution of the population of the enol, cyclized and *trans*-keto forms of Habs during each step of the (a) thermal relaxation study (see Figure 9) and of the (b) photochemical relaxation study (see Figure 10). Populations have been fixed arbitrarily.

zole rings, which replaces the intermolecular H-bond between the OH function and the triazole ring noted in Hsaltrz. We observe the formation of supramolecular double chains made by π–π stacking interactions with highly twisted molecules. Because of the absence of stacking of salicyl rings, Hsaltz can be classified as an open structure[51] that is typical of photochromic compounds but no photochromism was observed at room temperature with the powder sample of this compound.

Ksaltz is an interesting molecule because of its similarity to Hsaltz from an electronic point of view. The main difference between Hsaltz and Ksaltz originates from the difference in the involved supramolecular interactions. In Hsaltz, N–H intermolecular H-bonds appear to be very important in contrast to the ionic interactions present in Ksaltz. In addition, the appearance of ions leads to a drastic change in the medium polarity, which can have a large influence on the photochromic behaviour.[68] Whereas the intramolecular H-bonding between the alcohol and imine functions is similar in both structure, the Ksaltz structure contains planar molecules [Φ_1 = 6(1)°] although Hsaltz is constituted of highly twisted ones [Φ_1 = 35(1)°]. In addition to structural differences and, more precisely, to supramolecular network linkers, the major change between both compounds is observed in absorption optical properties. Ksaltz is shown to be strongly thermochromic, whereas Hsaltz is only slightly thermochromic. Surprisingly, this difference, associated to stabilization of the *cis*-keto form with respect to the enol form, is not correlated to a difference in intramolecular H-bonding strength. No change in emission properties is observed between both tetrazole compounds. Finally, Hsalphen appears to be similar to Habs due to its crystal packing directed by strong π–π stacking interactions. The highly close structure obtained is typical of thermochromic compounds[35] except that the dihedral angle is large [Φ_1 = 48(1)°]. The π–π stacking interactions seem to decrease the photochromism at room temperature but do not quench it. This observation is supported by the height of the energy barrier predicted by our calculations.

Fluorimetry on solid samples is a very interesting method to analyze *N*-salicylidene aniline derivatives because of their strong fluorescence, which allows probing energy levels involved during the photochemical processes. All molecules have a strong emission around 540 nm (from 523 to 569 nm) that can be attributed to the radiative relaxation of the excited *cis*-keto form. Habs and Hsalphen have more bathochromic emissions, whereas Hsaltrz has a more energetic emission (523 nm). This phenomenon can be attributed to the enlarged electronic conjugation generated by the presence of pyridine moieties in Habs and of aromatic rings placed side by side in Hsalphen. Interestingly, the emission of the enol form appears only in Hsaltrz and Hsalphen at very narrow wavelengths (438 and 441 nm, respectively). We thus suspect that the optical properties of the enol forms are less affected by described molecular changes than the ones of keto forms. We assume that the presence or the absence of enol emission is controlled by the energy gap between excited enol and *cis*-keto form levels.[42] Indeed, if this gap is large, as predicted by our calculations for Habs, excited enol molecules are very rapidly relaxed to the excited *cis*-keto form by tautomerism, which quenches the enol emission (Figure 1b).

Conclusions

We have presented new compounds that represent rare examples of thermo- and photochromic azole-based molecules. A supramolecular approach was used to select these new *N*-salicylidene aniline derivatives and to gain better control of the intermolecular interactions present in their molecular packings. Crystal engineering was developed with H-bonds (Hsaltrz and Hsaltz), π–π stacking (Habs and Hsalphen) and ionic interactions (Ksaltz) to build dense supramolecular networks. Electronic properties have been properly analyzed by computational means on isolated molecules and molecules incorporated into the real single-crystal packing. Optical properties in absorption and emission were then fully discussed and interesting links between the supramolecular interactions, electronic properties and the optical properties were fully discussed.

Starting from a nonfunctional molecule (Hsaltrz) that is neither thermochromic nor photochromic, chemical "sub-

stitutions" were made to lead to novel functional materials that are either thermochromic or photochromic. Hsaltz and Ksaltz are new thermochromic molecules where the thermosensibility is tuned by changing the type of supramolecular interactions (H-bonds–ionic interaction) and the medium polarity. Habs is a novel molecule that is exclusively photochromic. Our calculations show that this behaviour, hitherto not observed, can be explained by the high energy difference between the enol and *cis*-keto forms. Hsalphen appears to be thermochromic and photochromic although the packing is closed by the strong π–π stacking network. This strongly supports the idea that it is difficult to predict the optical properties of *N*-salicylidene aniline derivatives considering exclusively single-crystal packing analyses.[42] Energetic factors, properly analyzed by computational means, were then used to complete the optical properties prediction process.

Finally, Habs was presented as a highly interesting tristable molecule. In addition to the observed unstable *cis*-keto form, which is only photochemically accessible (observed by fluorimetry), the fundamental enol, the metastable *trans*-keto and cyclized forms were predicted by computational means. This new molecular scheme allows us to propose an explanation for the complex photochromic decay as well as the unexpected "spring-type" effect. The suggested complex kinetic scheme involved during thermal and photochemical relaxation was then presented and fully discussed in light of our computational study.

Experimental Section

Starting Materials: Solvents (absolute ethanol, chloroform and diethyl ether, analytical reagent and methanol HPLC grade from Prolabo; [D$_6$]DMSO 99.9 atom-%D, *n*-hexane HPLC grade from Aldrich and ethylene glycol 99% from Acros Organics) and reagents [4-amino-4*H*-1,2,4-triazole 99%, salicylaldehyde 99%, copper(II) chloride dehydrate 98%, 2-cyanopyridine 99%, hydrazine dihydrochloride 99% from Acros Organics; Sulfanilic acid 99%, (1,10)-phenanthrolin-5-amine 97%, hydrazine monohydrate 98%, 5-aminotetrazole 97% from Aldrich; potassium hydroxide analytical reagent from Riedel-de Haën and sodium hydroxide, analytical reagent from Fisher Scientific] were obtained commercially and used as received.

Sodium Salt of *N*-Salicylidene *para*-Aminobenzenesulfonate (Nasalsulfo): Prepared as a precursor for single-crystals growing of Hsaltrz. Sulfanilic acid (5 g, 28.8 mmol, 1 equiv.) was suspended in methanol (50 mL) and deprotonated by adding solid sodium hydroxide (1.16 g, 28.8 mmol, 1 equiv.) under reflux for 1 h. Afterwards, salicylaldehyde (3 mL, 28.8 mmol, 1 equiv.) was added to the white suspension to give a yellow solution. The mixture was stirred for 2 h at room temperature and then concentrated. The resulting solution was filtered to give 11.94 g of a crystalline yellow product that was washed with methanol (10 mL) and dried under vacuum. The pure product (7.44 g, 86%) was obtained after recrystallization in hot methanol (100 mL). ^{1}H NMR (300 MHz, [D$_6$]DMSO, 298 K): δ = 13.06 (s, 1 H, O*H*), 9.00 (s, 1 H, C*H*=N), 7.70 (m, 3 H, C*H*-C-CH=N and C*H*-CSO$_3$), 7.42 (m, 3 H, C*H*-CH-OH and C*H*-CH-SO$_3$), 7.00 (m, 2 H, C*H*-OH and C*H*-CH-CH-OH) ppm. ^{13}C NMR (300 MHz, [D$_6$]DMSO, 298 K): δ = 164.47 (*C*-OH), 161.05 (*C*H=N), 148.73 (*C*-N), 147.61 (*C*-SO$_3$), 134.14 (*C*H-CH-C-OH), 133.37 (*C*H-C-C-OH), 127.54 (*C*H-C-SO$_3$), 121.44 (*C*H-C-N), 120.07 (*C*-C-OH), 119.94 (*C*H-CH-CH-C-OH), 117.36 (*C*H-C-OH) ppm. $C_{13}H_{10}NNaO_4S$ (299.28): calcd. C 52.17, H 3.61, N 4.68, S 10.71; found C 52.31, H 3.30, N 4.40, S 10.47. MS: *m*/*z* (%) = 276 [M$^-$], 212 [M$^-$ – SO$_2$], 196 [M$^-$ – SO$_3$], 118 [$C_7H_4NO^-$]. X-ray powder diffraction: 3.24 (s), 6.42 (m), 9.64 (s), 12.8 (w), 16.04 (w), 18.38 (w), 19.67 (s), 20.81 (w), 21.68 (w), 23.30 (w), 23.58 (w), 25.40 (w), 25.80 (w), 27.08 (w), 25.80 (w), 26.00 (w), 27.08 (w), 30.34 (w), 31.12 (w), 32.40 (w), 32.62° (w). FTIR (KBr disk): $\tilde{\nu}$ = 418 (w), 442 (w), 459 (w), 494 (w), 528 (w), 552 (m), 565 (m), 577 (s), 634 (m), 650 (s), 716 (s), 731 (s), 779 (w), 812 (m), 835 (s), 850 (s), 912 (m), 935 (w), 982 (m), 1011 (m), 1032 (m), 1051 (s), 1107 (m), 1032 (s), 1150 (m), 1174 (s), 1186 (s), 1236 (s), 1261 (w), 1281 (s), 1319 (w), 1362 (m), 1404 (m), 1456 (m), 1489 (s), 1528 (w), 1576 (s), 1591 (m), 1626 (s), 1664 (w), 3250 (m, br.) cm^{-1}.

***N*-Salicylidene 4-Amino-1,2,4-triazole (Hsaltrz):** A solution of salicylaldehyde (1.25 mL, 1.18 mmol, 1 equiv.) dissolved in ethanol (5 mL) was added to a solution of 4-amino-1,2,4-triazole (1 g, 1.18 mmol, 1 equiv.) in ethanol (5 mL). The resulting slightly yellow solution was stirred for 15 min and, afterwards, heated at reflux for 45 min. The resulting pale-yellow solution was allowed to cool to room temperature to give a crystalline white powder. The product was filtered, washed with ethanol (1 mL) and ethyl ether (1 mL) and dried under vacuum (2 g, 90%). ^{1}H NMR (300 MHz, [D$_6$]DMSO, 298 K): δ = 10.50 (s, 1 H, H^{14}), 9.20 (m, 3 H, H^3, H^5 and H^7), 7.63 (m, 1 H, H^{13}), 7.46 (m, 1 H, H^{11}), 7.01 (m, 2 H, H^{10} and H^{12}) ppm. ^{13}C NMR (300 MHz, [D$_6$]DMSO, 298 K): δ = 158.93 (C^9), 155.71 (C^7), 139.76 (C^3 and C^5), 134.70 (C^{11}), 128.50 (C^{13}), 120.45 (C^{10}), 118.99 (C^8), 117.52 (C^{12}) ppm. $C_9H_8N_4O$ (188.19): calcd. C 57.44, H 4.28, N 29.77; found C 57.44, H 4.30, N 29.80. M.p. onset temperature by DSC: 206(1) °C. Degradation temperature (onset) by DSC: 220(1) °C. MS: *m*/*z* = 189 [M + H$^+$], 120 [$C_7H_6NO^{\cdot+}$], 70 [$C_2N_3H_5^{\cdot+}$]. X-ray powder diffraction: 7.86 (s), 9.48 (m), 11.72 (m), 14.26 (m), 14.86 (s), 15.78 (m), 16.2 (w), 17.0 (m), 16.88 (w), 18.06 (w), 18.78 (w), 19.08 (s), 19.84 (m), 20.48 (w), 21.2 (m), 22.06 (m), 22.76 (m), 23.74 (w), 26.1 (w), 28.38 (w), 28.8 (w), 28.7 (w), 30.96 (w), 34.94° (w). FTIR (KBr disk): $\tilde{\nu}$ = 461 (m), 515 (w), 598 (s), 623 (s), 729 (w), 762 (s), 833 (w), 854 (m), 949 (w), 974 (w), 1057 (s), 1105 (w), 1155 (s), 1194 (m), 1259 (s), 1300 (s), 1373 (m), 1412 (w), 1456 (s), 1516 (s), 1605 (s), 2710 (s, br.), 3117 (s), 3435 (s, br.) cm^{-1}. Single crystals were obtained following an unconventional procedure: Nasalsulfo (0.30 g, 1 mmol, 2 equiv.) was added to a solution of $CuCl_2 \cdot 2H_2O$ (0.12 g, 0.5 mmol, 1 equiv.) in methanol (10 mL). 4-Amino-1,2,4-triazole (0.13 g, 1.5 mmol, 3 equiv.), dissolved in methanol (10 mL), was allowed to slowly diffuse into the copper solution through a diffusion H-tube filled with methanol (100 mL). After 1 year, diffusion was assumed to be complete and the whole solution was allowed to slowly evaporate at room temperature. Long uncolored needles of diffractable quality were obtained within the resulting concentrated green solution after 6 months. These crystals were then analyzed by X-ray diffraction.

4-Amino-3,5-bis(pyridine-2-yl)-1,2,4-triazole (abpt): Obtained by following a reported procedure.[75] Yield: 2.76 g (55%). ^{1}H NMR (300 MHz, [D$_6$]DMSO, 298 K): δ = 8.78 (m, 2 H, H^{17} and H^{23}), 8.24 (m, 2 H, H^{20} and H^{26}), 8.08 (dt, *J* = 7.8, 1.77 Hz, 2 H, H^{19} and H^{25}), 7.83 (s, 2 H, N*H*$_2$), 7.59 (m, 2 H, H^{18} and H^{24}) ppm. ^{13}C NMR (300 MHz, [D$_6$]DMSO, 298 K): δ = 149.67 (C^{23} and C^{17}), 149.52 (C^3 and C^5), 147.78 (C^{15} and C^{21}), 138.52 (C^{19} and C^{25}), 125.30 (C^{18} and C^{24}), 123.55 (C^{20} and C^{26}) ppm.

***N*-Salicylidene 4-Amino-3,5-bis(pyridine-2-yl)-1,2,4-triazole (Habs):** abpt (2.5 g, 10.5 mmol, 1 equiv.) was dissolved in hot methanol

(25 mL) to give a clear solution, to which was added salicylaldehyde (1.1 mL, 10.5 mmol, 1 equiv.) to afford a clear pale-yellow solution. The mixture was heated at reflux for 48 h and then allowed to cool down to room temperature. The resulting crystalline yellow precipitate was filtered and recrystallized from hot methanol (60 mL) to give the pure product (2.58 g, 7.5 mmol, 72%). ^{1}H NMR (300 MHz, [D$_6$]DMSO, 298 K): δ = 10.66 (s, 1 H, H^{14}), 8.98 (s, 1 H, H^7), 8.66 (m, 2 H, H^{20} and H^{26}), 8.18 (d, J = 7.89 Hz, 2 H, H^{17} and H^{23}), 8.06 (dt, J = 7.76, 1.69 Hz, 2 H, H^{19} and H^{25}), 7.59 (m, 3 H, H^{12}, H^{18} and H^{24}), 7.47 (dt, J = 7.80, 1.68 Hz, 1 H, H^{11}), 6.97 (m, 2 H, H^{10} and H^{13}) ppm. ^{13}C NMR (300 MHz, [D$_6$]-DMSO, 298 K): δ = 168.30 (C^7), 159.54 (C^9), 150.65 (C^{15} and C^{21}), 150.34 (C^{20} and C^{26}), 147.29 (C^3 and C^5), 138.48 (C^{19} and C^{25}), 135.40 (C^{11}), 130.48 (C^{18} and C^{24}), 125.76 (C^{17} and C^{23}), 125.33 (C^{12}), 120.61 (C^{13}), 118.52 (C^{10}), 117.74 (C^8) ppm. $C_{19}H_{14}N_6O$ (342.36): calcd. C 66.66, H 4.12, N 24.55; found C 66.34, H 4.06, N 24.68. MS: m/z = 343 [M + H$^+$], 224 [$C_{12}H_{10}N_5$]. FTIR (KBr disk): $\tilde{\nu}$ = 472 (w), 554 (w), 604 (m), 623 (m), 642 (m), 690 (s), 731 (w), 739 (s), 760 (s), 787 (s), 914 (w), 895 (w), 910 (m), 964 (w), 993 (m), 1036 (w), 1091 (w), 1115 (w), 1150 (m), 1196 (m), 1254 (w), 1271 (s), 1367 (m), 1406 (m), 1429 (s), 1448 (s), 1460 (s), 1487 (s), 1519 (w), 1568 (s), 1587 (s), 1622 (s), 3040 (m), 3153 (m, br.) cm^{-1}. M.p. onset temperature by DSC: 161(1) °C. Degradation temperature by TGA (onset point): 261(1) °C. X-ray powder diffraction: 4.92 (w), 7.86 (s), 9.9 (m), 10.62 (m), 14.48 (w), 14.88 (m), 15.34 (w), 16.1 (s), 18.2 (m), 18.96 (m), 19.8 (w), 21.3 (w), 23.18 (m), 24.16 (w), 24.88 (w), 26.1 (w), 32.54 (w), 34.3 (w), 35.1 (w), 38.34 (w), 39.84 (w), 42.68 (w), 45.14 (m), 45.32 (w), 51.28° (w). Single crystals were obtained by sublimation under reduced pressure (110 °C, over a period of 3 months) on the cold finger condenser of a sublimator setup.

***N*-Salicylidene (1,10)-Phenanthrolin-5-amine (Hsalphen):** (1,10)-Phenanthrolin-5-amine (0.5026 g, 2.6 mmol, 1 equiv.) was dissolved in hot methanol (15 mL). Salicylaldehyde (3 mL, 28.5 mmol, 11 equiv.) was added to give a pale-yellow solution. The mixture was heated at reflux for 16 h and then allowed to cool to room temperature. The unreacted (1,10)-phenanthrolin-5-amine was filtered, and the solvent was removed under vacuum. The residual yellow oil was triturated with hexane (20 mL) and sonicated for 30 min. The supernatant containing an excess amount of salicylaldehyde was pipetted out without disturbing the oil. After repeating 6×, a pure yellow precipitate (0.6638 g, 2.21 mmol, 86%) was isolated from the oil, filtered and dried under vacuum. ^{1}H NMR (300 MHz, [D$_6$]DMSO, 298 K): δ = 12.37 (s, 1 H, H^{23}), 9.21 (d, J = 1.68 Hz, 1 H, H^9), 9.20 (s, 1 H, H^{16}), 9.09 (dd, J = 4.32, 1.71 Hz, 1 H, H^2), 8.70 (dd, J = 8.28, 1.71 Hz, 1 H, H^7), 8.52 (dd, J = 8.13, 1.68 Hz, 1 H, H^4), 7.89 (m, 3 H, H^6, H^8 and H^{18}), 7.81 (m, 1 H, H^3), 7.53 (m, 1 H, H^{21}), 7.08 (m, 2 H, H^{19} and H^{20}) ppm. ^{13}C NMR (300 MHz, [D$_6$]DMSO, 298 K): δ = 165.10 (C^{16}), 160.87 (C^{22}), 151.20 (C^9), 150.12 (C^2), 146.48 (C^5), 145.64 (C^{11}), 145.34 (C^{12}), 136.96 (C^4), 134.81 (C^{21}), 132.77 (C^{18}), 132.44 (C^7), 129.40 (C^{14}), 125.83 (C^{13}), 124.46 (C^6), 124.31 (C^3), 120.76 (C^{17}), 120.33 (C^{20}), 117.54 (C^{19}), 113.72 (C^8) ppm. MS: m/z = 300 [M + H$^+$], 599 [M$_2$], 322 [M + Na], 621 [M$_2$ + Na], 107 [C_7H_7O]. FTIR (KBr disk): $\tilde{\nu}$ = 517 (w), 565 (w), 608 (w), 621 (w), 656 (w), 702 (w), 742 (s), 752 (m), 781 (w), 806 (w), 833 (w), 881 (w), 893 (w), 922 (w), 991 (w), 1024 (w), 1036 (w), 1059 (m), 1084 (w), 1115 (w), 1140 (w), 1151 (w), 1197 (w), 1275 (s), 1300 (w), 1366 (w), 1394 (m), 1420 (m), 1460 (w), 1481 (w), 1560 (m), 1574 (m), 1601 (s), 1616 (s), 3022 (w, br.), 3448 (w, br.) cm^{-1}. M.p. onset temperature by DTA: 185(1) °C. Degradation temperature by DTA (onset point): 254(1) °C. $C_{19}H_{13}N_3O$ (299.10): calcd. C 76.23, H 4.38, N 14.04; found C 75.35, H 4.19, N 13.40. X-ray powder diffraction: 7.72 (s), 11.38 (m), 11.7 (s), 12.7 (w), 13.42 (w), 14.24 (w), 14.94 (w), 15.4 (m), 15.98 (m), 16.74 (m), 17.08 (m), 17.54 (m), 18.36 (m), 18.96 (m), 19.8 (s), 20.28 (w), 20.32 (w), 21.6 (m), 22.1 (m), 22.44 (m), 23.44 (s), 24.58 (m), 25 (m), 26.4 (s), 27.36 (s), 28.26 (w), 28.68 (w), 29.34 (m), 30.06 (w), 31.92 (w), 33.02 (w), 33.56 (w), 34.36 (w), 37.96 (w), 38.86° (w). White single crystals of X-ray quality were obtained by slow evaporation of a saturated solution in ethyl ether.

***N*-Salicylidene 5-Aminotetrazole (Hsaltz):** Synthesis was performed under a dried argon atmosphere. 5-Aminotetrazole (5.0023 g, 58.8 mmol, 1 equiv.) was degassed under vacuum. Ethanol (50 mL), dried and kept over molecular sieves, was bubbled with argon for 30 min. 5-Aminotetrazole was dissolved in hot ethanol by using Schlenk techniques. Salicylaldehyde was slowly added, leading to a pale-green solution. The mixture was heated at reflux for 5 h under an atmosphere of argon and then filtered, washed with a few milliliters of degassed and dried ethanol and then dried under vacuum. The resulting yellow precipitate was suspended in ethyl ether (75 mL) and sonicated in an ultrasonic bath for 1 h. The pure product (6 g, 31.7 mmol, 54%) was obtained and dried under vacuum. ^{1}H NMR (300 MHz, [D$_6$]DMSO, 298 K): δ = 11.52 (s, 1 H, H^{14}), 9.53 (s, 1 H, H^7), 7.92 (d, J = 7.32 Hz, 1 H, H^{13}), 7.52 (t, J = 7.23 Hz, 1 H, H^{11}), 7.03 (m, 2 H, H^{10} and H^{12}), 6.48 (s, 1 H, H^4) ppm. ^{13}C NMR (300 MHz, [D$_6$]DMSO, 298 K): δ = 167.79 (C^7), 162.64 (C^9), 161.35 (C^5), 157.60 (C^8), 136.39 (C^{11}), 131.45 (C^{13}), 120.70 (C^{12}), 117.90 (C^{10}) ppm. MS: m/z = 190 [M], 162 [M – N$_2$]. X-ray powder diffraction: 7.40 (w), 8.98 (s), 10.38 (w), 10.48 (w), 12.34 (w), 12.48 (w), 13.92 (w), 14.64 (w), 15.88 (m), 16.86 (w), 17.82 (w), 19.00 (m), 20.16 (m), 20.28 (w), 21.44 (w), 22.98 (w), 23.56 (m), 23.74 (w), 24.34 (w), 25.28 (m), 25.16 (w), 26.60 (m), 27.12 (m), 27.84 (w), 28.32 (m), 28.38 (m), 29.1 (w), 31.56 (w), 35.48° (w). White single crystals of good quality were obtained by slow evaporation of a saturated solution of ethyl ether.

Potassium Salt of *N*-Salicylidene 5-Aminotetrazolate (Ksaltz): In a first step, 5-aminotetrazole (2.51 g, 29.5 mmol, 1 equiv.) was dissolved in distilled water (50 mL). Potassium hydroxide pellets (1.66 g, 29.5 mmol, 1 equiv.) were slowly added to the solution. The mixture was heated at reflux overnight, concentrated under vacuum and then the resulting white precipitate was dried (3.9332 g, 78%). The product was dissolved in methanol (50 mL) and salicylaldehyde (3.36 mL, 32 mmol, 1 equiv.) were added. The mixture was heated at reflux overnight to give a clear yellow solution, which was concentrated under vacuum. The crude product contained 10% of unreacted salicylaldehyde. This mixture was sonicated (3×) with hexane (50 mL) to give the pure product (5.51 g, 76%). Data for the potassium salt of 5-aminotetrazolate: ^{1}H NMR (300 MHz, [D$_6$]-DMSO, 298 K): δ = 4.73 (s, 2 H, NH_2) ppm. ^{13}C NMR (300 MHz, [D$_6$]DMSO, 298 K): δ = 163.68 (*C*-NH$_2$) ppm. Data for Ksaltz: ^{1}H NMR (300 MHz, [D$_6$]DMSO, 298 K): δ = 13.25 (br. s, 1 H, H^1), 9.35 (s, 1 H, H^8), 7.72 (dd, J = 7.98, 1.50 Hz, 1 H, H^6), 7.43 (dt, J = 7.30, 1.62 Hz, 1 H, H^4), 6.98 (m, 2 H, H^3 and H^5) ppm. ^{13}C NMR (300 MHz, [D$_6$]DMSO, 298 K): δ = 166.06 (C^2), 163.04 (C^8), 160.97 (C^9), 133.64 (C^4), 132.78 (C^6), 119.98 (C^7), 119.71 (C^5), 117.13 (C^3) ppm. MS: m/z = 188 [M]. $C_8H_6KN_5O$ (227.27): calcd. C 42.28, H 2.66, N 30.82; found C 42.92, H 2.73, N 31.14. X-ray powder diffraction: 13.34 (w), 13.86 (w), 14.80 (m), 15.44 (s), 16.46 (w), 18.52 (s), 18.84 (w), 19.82 (w), 20.68 (w), 22.58 (w), 23.22 (m), 24.26 (m), 25.40 (m), 26.86 (s), 27.80 (s), 28.82 (s), 29.00 (w), 30.48 (w), 31.84 (w), 33.16 (w), 34.7 (w), 36.66 (m), 42.2 (w), 43.68 (m), 45.12 (w), 46.50 (w), 48.42 (w), 49.64 (w), 50.62° (w). Yellow single crystals of good quality were obtained by slow evaporation of a saturated solution in methanol. X-ray diffraction measurements were done at room temperature because of the instability of crystals at low temperature (120 K).

Instrumentation: Sonication was performed with a Branson 3510 ultrasonic bath. ^{1}H and ^{13}C NMR spectra were recorded with a Bruker AC 300 MHz instrument with the DMSO proton peak as internal standard. Peaks assignments for Hsaltrz, Habs, Hsalphen, Hsaltz and Ksaltz NMR spectra were carried out by using atomic numbering from CIF files. Peaks assignments in abpt NMR spectra were made by using the same atomic numbering as in the Habs CIF file. Mass spectroscopic data were obtained with a Thermofinnigan LCQ ion trap spectrometer by using an ESI ionization mode for Hsaltz and Hsalphen and APCI ionization mode for Habs and Hsaltrz. Infrared spectra were recorded with a Shimadzu FTIR-8400S spectrometer with KBr disks. Elementary analyses were performed at University College London. The TGA/DTA instrument used was a TA instrument SDT2960 Simultaneous DSC-TGA with alumina crucibles filled with approximately 10 mg of sample. Approximately 10 mg of dried aluminium oxide were used as reference for DTA measurements. DSC measurements were carried out at a scanning rate of 10 K/min, over the temperature range (298–873 K) with a Mettler Toledo DSC20, calibrated with pure aluminium (s/l) and indium (s/l), and with alumina sample holders. X-ray powder diffractograms were performed with a Siemens D5000 X-ray diffractometer, with a Cu anticathode ($\lambda_{K\text{-}\alpha}$ = 1.5418 Å) in Bragg–Brentano geometry (θ/θ mode). Samples were deposited on silicon after calibration with a quartz standard. Diffuse reflectance spectra were obtained with a Varian Cary 5E spectrometer by using PTFE as a reference. Spectra were measured on pure solids to avoid matrix effects.[48,57–68] Eventual distortions in the Kubelka Munk spectra[76] that could result from the study of pure compounds have not been considered because no comparison with absorption spectra was necessary. Solid-state emission spectra were obtained with a Fluorolog-3 (Jobin–Yvon-Spex Company) spectrometer. Kubelka Munk and emissions spectra were normalized to allow meaningful comparisons. Light irradiations were carried out with a standard lamp used for visualizing TLC plates (ROC; intensity at 15 cm from filter: 440 μW cm^{-2} at 254 nm). The reversibility of the *cis–trans* isomerization was checked with a LOT-ORIEL 200 W high-pressure mercury arc lamp combined with a water cooling setup to avoid infrared light exposure. In situ irradiations were carried out for 10 min with appropriate filters. Data that were accumulated each 30 s were normalized.

X-ray Structure Data Collection and Refinement: For Hsaltrz, Habs, Hsalphen and Hsaltz, X-ray intensity data were collected at 120 K with a MAR345 image plate using Mo-K_α (λ = 0.71069 Å) radiation. The crystal was chosen, mounted in inert oil and transferred quickly to the cold gas stream for flash cooling. For Ksaltz, the data were collected at room temperature with a Xcalibur CCD diffractometer (Gemini ultra Mo) using Mo-K_α (λ = 0.71069 Å) radiation. Crystal data and data collection parameters are summarized in Table S1 (Supporting Information). The unit cell parameters were refined using all collected spots after the integration process. Except for Ksaltz, the data were not corrected for absorption, but the data collection mode partially takes the absorption phenomena into account. (See the total number of collected reflections vs. the independent number of reflections in Table S1, Supporting Information). The five structures were solved by direct methods with SHELX97.[77] All the structures were refined by full-matrix least-squares on F^2 using SHELX97.[77] All the non-hydrogen atoms were refined with anisotropic temperature factors. For Hsaltrz, Habs, Hsalphen and Hsaltz, all hydrogen atoms were localized by Fourier-difference synthesis. For Ksaltz, only H1 of the hydroxy group was localized, the other H atoms were calculated with AFIX. The H atoms were included in the refinement with a common isotropic temperature factor. The details of the refinement and the final *R* indices are presented in Table S1 (Supporting Information). CCDC-748023 (for Hsalphen), -748024 (for Habs), -748025 (for Hsaltz), -748026 (for Ksaltz) and -748027 (for Hsaltrz) contain the supplementary crystallographic data for this paper. These data can be obtained free of charge from the Cambridge Crystallographic Data Centre via www.ccdc.cam.ac.uk/data_request/cif.

Computational Methods: For isolated molecules, the geometry optimization of the ground and excited states was performed at the UB3LYP/6-31G(d,p) and CIS/6-31G(d,p) levels of theory, respectively, using Jaguar 6.5 pseudospectral program package.[78] Enol, *cis*-keto and *trans*-keto forms and cyclized intermediate (in the case of Habs) were fully geometry optimized. Energy profile for *cis*-keto/*trans*-keto isomerization was obtained by performing a set of constrained geometry optimization at successively lower values of the C^4–C^3–C^2–N^1 torsion angle (see Scheme 2). All energies are given after single-point calculations at the CIS/6-31G(d) level using the Gaussian 03 program.[79]

For calculations taking crystal packing into account, systems were taken so as to be constituted of one molecule surrounded by others in every direction (4 and 5 for Habs and Hsalphen, respectively). Crystal environment created by neighbouring molecules was taken from X-ray crystal structures. Optimization was performed at the CIS/6-31G(d,p) level of theory (S^1). The position of every atom of such molecules was frozen during optimization calculations with only the central molecule being fully geometry optimized, excepted for the intermediates during *cis*-keto/*trans*-keto isomerization, which were obtained by freezing the C^4–C^3–C^2–N^1 torsion angle (see Scheme 2) at successive values of this torsion angle. Energies were obtained by single-point calculations with the central molecule and crystal packing (surrounding molecules) treated at the B3LYP/6-31G(d) and B3LYP/6-31G level of theory, respectively. Stabilization energy induced by the packing was estimated by Equation (1).

$$E_{stab} = E_{system} - E_{isolated\ molecule} - E_{surrounding\ molecules} \quad (1)$$

where E_{system} is the energy of the full system (i.e., central molecule and surrounding molecules), $E_{isolated}$ molecule is the energy [B3LYP/6-31G(d)] of the central molecule of interest without its surrounding, $E_{surrounding\ molecules}$ is the energy (B3LYP/6-31G) of the surrounding molecules (without the molecule of interest). The relative stabilization energy respective to the enol form was estimated according to Equation (2).

$$\text{rel. } E_{stab} = E_{stab}^{intermediate} - E_{stab}^{enol} \quad (2)$$

Calculations of interaction energies are susceptible to basis set superposition error (BSSE). In order to eliminate this error, $E_{isolated}$ molecule and $E_{surrounding\ molecules}$ were estimated by single-point calculations using a mixed basis set containing "ghost orbitals" corresponding to the surrounding molecules and the central molecule, respectively. The values of E_{stab} are available in Table S3 (Supporting Information).

Supporting Information (see footnote on the first page of this article): Crystal data and structure refinement data of the compounds studied; emission maximum wavelengths of the compounds; calculated energies for Habs and Hsalphen as isolated molecules and in the crystal packing; NPA charges for Habs; calculated structures and energies for Habs and Hsalphen; synthetic pathway leading to the growing of single crystals of Hsaltrz.

Acknowledgments

This work was partly funded by the Fonds Special de Recherche de l'Université Catholique de Louvain, the Fonds de la Recherche Scientifique-FNRS (FRFC project No.2.4508.08, No.2.4502.05 and No.2.4.511.07.F), the Interuniversity Attraction Pole IAP-VI (P6/17) INANOMAT program and the Concerted Research Action of the "Communauté Française de Belgique" allotted by the Académie Universitaire Louvain. We also thank the Fonds pour la Formation à la Recherche dans l'Industrie et dans l'Agriculture for a doctoral scholarship allocated to F.R and the FRS-FNRS for a Chargé de recherches position to R.R. We also thank B. Norberg for the X-ray data collection of Ksaltz.

[1] J.-M. Lehn, *Science* **2002**, *295*, 2400–2403.
[2] K. Ono, M. Yoshizawa, M. Akita, T. Kato, Y. Tsunobuchi, S. Ohkoshi, M. Fujita, *J. Am. Chem. Soc.* **2009**, *131*, 2782–2783.
[3] J. Qian, F. Wu, *Chem. Mater.* **2009**, *21*, 758–762.
[4] J. L. Li, X. Y. Liu, R.-Y. Wang, J.-Y. Xiong, *J. Phys. Chem. B* **2005**, *109*, 24231–24235.
[5] S. Goswami, S. Jana, S. Dey, I. A. Razak, H. K. Fun, *Supramol. Chem.* **2006**, *18*, 571–574.
[6] K. S. Suslick, N. A. Rakow, A. Sen, *Tetrahedron* **2004**, *60*, 11133–11138.
[7] M. E. Kosal, J.-H. Chou, S. R. Wilson, K. S. Suslick, *Nat. Mater.* **2002**, *1*, 118–121.
[8] N. Lin, A. Langner, S. L. Tait, C. Rajadurai, M. Ruben, K. Kern, *Chem. Commun.* **2007**, 4860–4862.
[9] A. Rochefort, E. Bayard, S. Hadj-Messaoudi, *Adv. Mater.* **2007**, *19*, 1992–1995.
[10] S. Yagai, T. Karatsu, A. Kitamura, *Chem. Eur. J.* **2005**, *11*, 4054–4063.
[11] A. Mukherjee, M. K. Saha, M. Nethaji, A. R. Chakravarty, *New J. Chem.* **2005**, *29*, 596–603.
[12] Y. Zakrevskyy, J. Stumpe, C. F. J. Faul, *Adv. Mater.* **2006**, *18*, 2133–2136.
[13] P. Metrangolo, F. Meyer, T. Pilati, G. Resnati, G. Terraneo, *Angew. Chem. Int. Ed.* **2008**, *47*, 6114–6127.
[14] M. Schmittel, V. Kalsani, J. W. Bats, *Inorg. Chem.* **2005**, *44*, 4115–4117.
[15] M. Barboiu, E. Petit, A. van der Lee, G. Vaughan, *Inorg. Chem.* **2006**, *45*, 484–486.
[16] J. I. van der Vlugt, S. Demeshko, S. Dechert, F. Meyer, *Inorg. Chem.* **2008**, *47*, 1576–1585.
[17] H. Sleiman, P. N. W. Baxter, J.-M. Lehn, K. Airola, K. Rissanen, *Inorg. Chem.* **1997**, *36*, 4734–4742.
[18] V. Chandrasekhar, L. Nagarajan, R. Clérac, S. Ghosh, S. Verma, *Inorg. Chem.* **2008**, *47*, 1067–1073.
[19] M. Kinoshita, *Int. J. Mol. Sci.* **2009**, *10*, 1064–1080.
[20] J. D. Crowley, B. Bosnich, *Eur. J. Inorg. Chem.* **2005**, 2015–2025.
[21] T. Weilandt, R. W. Troff, H. Saxell, K. Rissanen, C. A. Schalley, *Inorg. Chem.* **2008**, *47*, 7588–7598.
[22] K. Yamauchi, Y. Takashima, A. Hashidzume, H. Yamaguchi, A. Harada, *J. Am. Chem. Soc.* **2008**, *130*, 5024–5025.
[23] Z. Ge, J. Hu, F. Huang, S. Liu, *Angew. Chem. Int. Ed.* **2009**, *48*, 1798–1802.
[24] C. Rajadurai, F. Schramm, S. Brink, O. Fuhr, M. Ghafari, R. Kruk, M. Ruben, *Inorg. Chem.* **2006**, *45*, 10019–10021.
[25] P. A. N. Reddy, M. Nethaji, A. R. Chakravarty, *Inorg. Chem. Commun.* **2003**, *6*, 698–701.
[26] a) G. R. Desiraju, *The Crystal as a Supramolecular Entity* Wiley, Chichester, United Kingdom, **1996**; b) F. S. Delgado, C. Ruiz-Pérez, J. Sanchiz, F. Lloret, M. Julve, *CrystEngComm* **2006**, *8*, 530–544.
[27] A. Plaquet, M. Guillaume, B. Champagne, L. Rougier, F. Mançois, V. Rodriguez, J.-L. Pozzo, L. Ducasse, F. Castet, *J. Phys. Chem. C* **2008**, *112*, 5638–5645.
[28] C. Baleizão, H. Garcia, *Chem. Rev.* **2006**, *106*, 3987–4043.
[29] R. K. Parashar, R. C. Sharma, A. Kumar, G. Mohan, *Inorg. Chim. Acta* **1988**, *151*, 201–208.
[30] Z. Cimerman, N. Galic, B. Bosner, *Anal. Chim. Acta* **1997**, *343*, 145–153.
[31] F. D. Jochum, P. Theato, *Macromolecules* **2009**, *42*, 5941–5945.
[32] B. L. Feringa, *Acc. Chem. Res.* **2001**, *34*, 504–513.
[33] S. Kawata, Y. Kawata, *Chem. Rev.* **2000**, *100*, 1777–1788.
[34] B. L. Feringa, W. F. Jager, B. de Lange, *Tetrahedron* **1993**, *49*, 8267–8310.
[35] T. Fujiwara, J. Hadara, K. Ogawa, *J. Phys. Chem. B* **2004**, *108*, 4035–4038.
[36] D. S. Lo, D. M. Manikowski, M. M. Hanson, *Appl. Opt.* **1971**, *10*, 978–979.
[37] a) Y. Fukuda, *Inorganic Chromotropism, Basic Concepts and Applications of Colored Materials*, Springer, New York, **2007**; b) G. H. Brown, *Photochromism*, Wiley, New York, **1971**; c) H. Dürr, B. Laurent, *Photochromism: Molecules and Systems*, 2nd ed., Elsevier, Amsterdam, The Netherlands, **2003**; d) J. C. Crano, R. J. Guglielmetti, *Organic Photochromic and Thermochromic compounds*, Plenum, New York, **1998**.
[38] E. Hadjoudis, *Mol. Eng.* **1995**, *5*, 301–337.
[39] M. E. Kletskii, A. A. Millov, A. V. Metelitsa, M. I. Knyazhansky, *J. Photochem. Photobiol., A* **1997**, *110*, 267–270.
[40] N. Otsubo, C. Okabe, H. Mori, K. Sakota, K. Amimoto, T. Kawato, H. Sekiya, *J. Photochem. Photobiol., A* **2002**, *154*, 33–39.
[41] V. C. Vargas, *J. Phys. Chem. A* **2004**, *108*, 281–288.
[42] F. Robert, A. D. Naïk, B. Tinant, R. Robiette, Y. Garcia, *Chem. Eur. J.* **2009**, *15*, 4327–4342.
[43] O. Sato, *J. Photochem. Photobiol., C* **2004**, *5*, 203–223.
[44] T. He, J.-N. Yao, *J. Mater. Chem.* **2007**, *17*, 4547–4557.
[45] P. Gütlich, Y. Garcia, T. Woike, *Coord. Chem. Rev.* **2001**, *219–221*, 839–879.
[46] O. Sato, *Acc. Chem. Res.* **2003**, *36*, 692–700.
[47] J. Saltiel, T. S. R. Krishna, R. J. Clark, *J. Phys. Chem. A* **2006**, *110*, 1694–1697.
[48] K. Amimoto, T. Kawato, *J. Photochem. Photobiol., C* **2005**, *6*, 207–226.
[49] H. Tian, Y. Feng, *J. Mater. Chem.* **2008**, *18*, 1617–1622.
[50] E. Hadjoudis, M. Vittorakis, I. Moustakali-Mavridis, *Tetrahedron* **1987**, *43*, 1345–1360.
[51] E. Hadjoudis, I. Moustakali-Mavridis, *Chem. Soc. Rev.* **2004**, *33*, 579–588.
[52] T. Inabe, N. Hoshino, T. Mitani, Y. Maruyama, *Bull. Chem. Soc. Jpn.* **1989**, *62*, 2245–2251.
[53] I. Moustakali-Mavridis, E. Hadjoudis, A. Mavridis, *Acta Crystallogr., Sect. B* **1978**, *34*, 3709–3715.
[54] J. Bregman, L. Leiserowitz, K. Osaki, *J. Chem. Soc.* **1964**, 2086–2100.
[55] R. Destro, A. Gavezzotti, M. Simonetta, *Acta Crystallogr., Sect. B* **1978**, *34*, 2867–2869.
[56] a) F. Arod, M. Gardon, P. Pattison, G. Chapuis, *Acta Crystallogr., Sect. C* **2005**, *61*, o317–o320; b) F. Arod, P. Pattison, K. J. Schenk, G. Chapuis, *Cryst. Growth Des.* **2007**, *7/9*, 1679–1685.
[57] E. Hadjoudis, A. B. Bournilos, D. Petridis, *J. Inclusion Phenom. Macrocyclic Chem.* **2002**, *42*, 275–279.
[58] L. Z. Zhang, Y. Xiang, P. Cheng, G. Q. Tang, D. Z. Liao, *Chem. Phys. Lett.* **2002**, *358*, 278–283.
[59] M. Ziółek, I. Sobczak, *J. Inclusion Phenom. Macrocyclic Chem.* **2009**, *63*, 211–218.
[60] S. Sakagami, T. Koga, A. Takase, *Mol. Cryst. Liq. Cryst.* **2002**, *373*, 71–81.
[61] E. Hadjoudis, V. Verganelakis, C. Trapalis, G. Kordas, *Mol. Eng.* **1999**, *8*, 459–469.
[62] P. Xue, R. Lu, G. Chen, Y. Zhang, H. Nomoto, M. Takafuji, H. Ihara, *Chem. Eur. J.* **2007**, *13*, 8231–8239.
[63] P. Chen, R. Lu, P. Xue, T. Xu, G. Chen, Y. Zhao, *Langmuir* **2009**, *25*, 8395–8399.

[64] T. Kawato, H. Koyama, H. Kanatomi, K. Yonetani, H. Matsushita, *Chem. Lett.* **1994**, 665–668.
[65] G. Pistolis, D. Gegiou, E. Hadjoudis, *J. Photochem. Photobiol., A* **1996**, *93*, 179–184.
[66] E. Hadjoudis, T. Dziembowska, Z. Rozwadowski, *J. Photochem. Photobiol., A* **1999**, *128*, 97–104.
[67] T. Haneda, M. Kawano, T. Kojima, M. Fujita, *Angew. Chem. Int. Ed.* **2007**, *46*, 6643–6645.
[68] I. Casades, M. Alvaro, H. Garcia, M. N. Pillai, *Eur. J. Org. Chem.* **2002**, 2074–2079.
[69] E. Hadjoudis, J. Argyroglou, E. Lambi, I. Moustaki-Mavridis, *Mol. Eng.* **1991**, *1*, 67–74.
[70] E. Hadjoudis, J. Petrou, J. Xexakis, *Mol. Cryst. Liq. Cryst.* **1983**, *93*, 73–81.
[71] K. Ogawa, Y. Kasahara, Y. Otani, J. Harada, *J. Am. Chem. Soc.* **1998**, *120*, 7107–7108.
[72] Although the presence of polymorphs cannot be rejected, on the basis of the difference between simulated and experimental X-ray powder diffractograms, a very nice correspondence between optical and structural properties have been observed.
[73] Except for Hsalphen in the T^1 state
[74] These values are, however, only rough estimates of this stabilization and have to be taken with caution. Indeed, these calculations do not take into account the distortion of the surrounding molecules nor the crystal-packing dilatation.
[75] F. Bentiss, M. Lagrenée, D. Barbry, *Tetrahedron Lett.* **2000**, *41*, 1539–1541.
[76] K. Ogawa, J. Harada, T. Fujiwara, H. Takahashi, *Chem. Lett.* **2004**, *33*, 1446–1447.
[77] G. M. Sheldrick, *SHELX97: Program System for Crystal Structure Determination*, University of Göttingen, Germany, **1997**.
[78] *Jaguar*, version 6.5, Schrodinger, LLC, New York, **2005**.
[79] M. J. Frisch, G. W. Trucks, H. B. Schlegel, G. E. Scuseria, M. A. Robb, J. R. Cheeseman, J. A. Montgomery Jr., T. Vreven, K. N. Kudin, J. C. Burant, J. M. Millam, S. S. Iyengar, J. Tomasi, V. Barone, B. Mennucci, M. Cossi, G. Scalmani, N. Rega, G. A. Petersson, H. Nakatsuji, M. Hada, M. Ehara, K. Toyota, R. R. Fukuda, J. Hasegawa, M. Ishida, T. Nakajima, Y. Honda, O. Kitao, H. Nakai, M. Klene, X. Li, J. E. Knox, H. P. Hratchian, J. B. Cross, V. Bakken, C. Adamo, J. Jaramillo, R. Gomperts, R. E. Stratmann, O. Yazyev, A. J. Austin, R. Cammi, C. Pomelli, J. W. Ochterski, P. Y. Ayala, K. Morokuma, G. A. Voth, P. Salvador, J. J. Dannenberg, V. G. Zakrzewski, S. Dapprich, A. D. Daniels, M. C. Strain, O. Farkas, D. K. Malick, A. D. Rabuck, K. Raghavachari, J. B. Foresman, J. V. Ortiz, Q. Cui, A. G. Baboul, S. Clifford, J. Cioslowski, B. B. Stefanov, G. Liu, A. Liashenko, P. Piskorz, I. Komaromi, R. L. Martin, D. J. Fox, T. Keith, M. A. Al-Laham, C. Y. Peng, A. Nanayakkara, M. Challacombe, P. M. W. Gill, B. Johnson, W. Chen, M. W. Wong, C. Gonzalez, J. A. Pople, *Gaussian 03*, revision B.04, Gaussian, Inc., Pittsburgh, **2003**.

Received: October 16, 2009
Published Online: December 8, 2009

